JACS
JOURNAL OF THE AMERICAN CHEMICAL SOCIETY

Subscriber access provided by ISTANBUL TEKNIK UNIV

Article

Architectural Diversity and Elastic Networks in Hydrogen-Bonded Host Frameworks: From Molecular Jaws to Cylinders

Matthew J. Horner, K. Travis Holman, and Michael D. Ward

J. Am. Chem. Soc., **2007**, 129 (47), 14640-14660 • DOI: 10.1021/ja0741574

Downloaded from http://pubs.acs.org on February 9, 2009

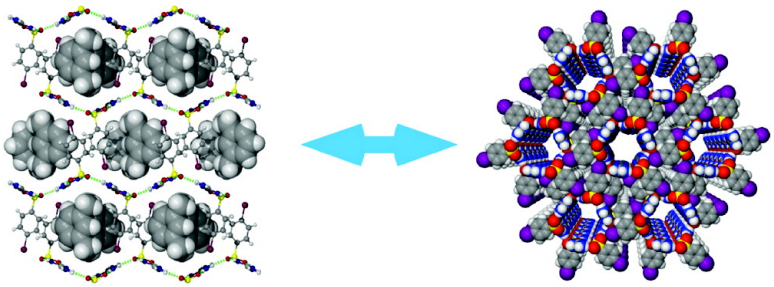

More About This Article

Additional resources and features associated with this article are available within the HTML version:

- Supporting Information
- Links to the 4 articles that cite this article, as of the time of this article download
- Access to high resolution figures
- Links to articles and content related to this article
- Copyright permission to reproduce figures and/or text from this article

View the Full Text HTML

ACS Publications
High quality. High impact.

Journal of the American Chemical Society is published by the American Chemical Society. 1155 Sixteenth Street N.W., Washington, DC 20036

J|A|C|S
ARTICLES
Published on Web 11/07/2007

Architectural Diversity and Elastic Networks in Hydrogen-Bonded Host Frameworks: From Molecular Jaws to Cylinders

Matthew J. Horner,[§] K. Travis Holman,[‡] and Michael D. Ward*,[†]

Contribution from the Department of Chemistry and the Molecular Design Institute, New York University, 100 Washington Square East, New York, New York 10003-6688, and the Department of Chemistry, Georgetown University, Washington, D.C. 20057

Received June 7, 2007; E-mail: mdw3@nyu.edu

Abstract: Guest-free guanidinium organomonosulfonates (GMS) and their inclusion compounds display a variety of lamellar crystalline architectures distinguished by different "up−down" projections of the organomonosulfonate residues on either side of a two-dimensional (2D) hydrogen-bonding network of complementary guanidinium ions (G) and sulfonate moieties (S), the so-called GS sheet. Using a combinatorial library of 24 GMS hosts and 26 guest molecules, a total of 304 inclusion compounds out of a possible 624 possible host−guest combinations were realized, revealing a remarkable capacity of the GMS hosts to form inclusion compounds despite the facile formation of the corresponding guest-free compounds and the absence of "predestined" inclusion cavities like those in related guanidinium organo*di*sulfonate host frameworks. The GS sheets in the inclusion compounds behave as "molecular jaws" in which organomonosulfonate groups projecting from opposing sheets clamp down on the guest molecules, forming ordered interdigitated arrays of the host organic groups and guests. Both the guest-free and inclusion compounds display a variety of architectures that reveal the structural integrity of two-dimensional GS sheet and the unique ability of these hosts to conform to the steric demands of the organic guests. Certain GMS host−guest combinations prompt formation of tubular inclusion compounds in which the GS sheet curls into cylinders with retention of the 2D GS network. The cylinders assemble into hexagonal arrays through interdigitation of the organosulfonate residues that project from their outer surfaces, crystallizing in high-symmetry trigonal or hexagonal space groups. This unique example of network curvature and structural isomerism between lamellar and cylindrical structures, with retention of supramolecular connectivity, is reminiscent of the phase behavior observed in surfactant microstructures and block copolymers. The large number of host−guest combinations explored here permits grouping of the inclusion compound architectures according to the shape of the guests and the relative volumes of the organomonosulfonate groups, enabling more reliable structure prediction for this class of compounds than for molecular crystals in general.

Introduction

The delicate and noncovalent nature of intermolecular forces responsible for packing in molecular crystals often frustrates solid-state design, which in turn limits the synthesis of functional materials. Computational methods for complete crystal structure prediction, including space group, lattice parameters, and atomic positions, continue to improve, but the lattice energy of different calculated forms of the same compound can differ by as little as a few kJ mol^{-1}, making an unambiguous assignment of the lowest energy structure difficult.[1,2] Indeed, the complexity of crystal packing forces has been compared to that of protein folding, and even the most innocent structural modification to a molecular constituent can lead to a completely unanticipated solid-state structure.[3,4] This has prompted the development of empirical guidelines for steering molecular assembly into prescribed crystal architectures based on well-defined structure-directing interactions, such as hydrogen bonding or metal coordination, which can override the cumulative effect of the multitude of weaker forces, such as van der Waals interactions. In this manner, lattice architectures often can be anticipated from the symmetry of the molecular building blocks and the propagation of bonding between the structure-directing groups. Although empirical guidelines rarely lead to complete and precise structure prediction, architectures based on supramolecular networks that are robust toward the introduction of ancillary groups can permit systematic and rational manipulation of solid-state structure.[5−13]

[§] Ph.D. thesis, University of Minnesota.
[‡] Georgetown University.
[†] New York University.

(1) Gavezzottti, A. *Acc. Chem. Res.* **1994**, *27*, 309.
(2) Dunitz, J. D.; Gavezzotti, A. *Angew. Chem. Int. Ed.* **2005**, *44*, 1766.
(3) Dunitz, J. D. *Chem. Commun.* **2003**, 545.
(4) Dunitz, J. D.; Scheraga, H. A. *Proc. Natl. Acad. Sci. U.S.A.* **2004**, *102*, 14309.
(5) (a) Yaghi, O. M.; O'Keeffe, M.; Ockwig, N.; Chae, H. K.; Eddaoudi, M.; Kim, J. *Nature* **2003**, *423*, 705. (b) Rowsell, J.; Millward, A.; Park, K.; Yaghi, O. M. *J. Am. Chem. Soc.* **2004**, *126*, 5666.

10.1021/ja0741574 CCC: $37.00 **© 2007 American Chemical Society**

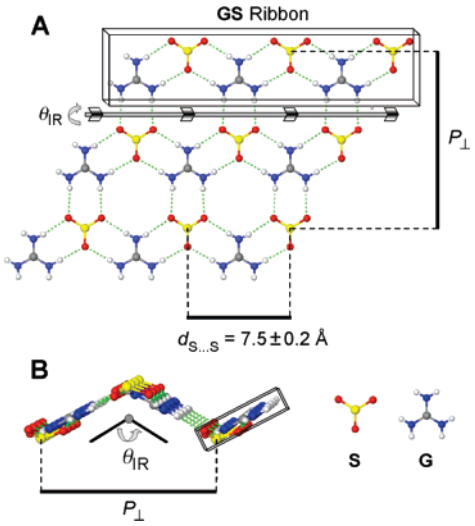

Figure 1. (A) The 2-D sheet formed by hydrogen bonds between the complementary guanidinium (G) ions and organosulfonates (S). (B) A typical GS sheet as viewed along the ribbon direction, illustrating the conformational flexibility of the hydrogen-bonded GS network that leads to accordion-like puckering in lamellar architectures.

Our laboratory has reported a series of crystalline materials based on guanidinium cations (G = $(C(NH_2)_3^+$) and the sulfonate moieties of organomonosulfonates (S = R−SO_3^-) or organodisulfonate anions (S = ^-O_3S−R−SO_3^-). The threefold symmetry and hydrogen-bonding complementarity of the G ions and S moieties prompt the formation of a two-dimensional (2D) quasi-hexagonal hydrogen-bonding network (Figure 1), which has proven to be remarkably robust toward the introduction of various organic pendant groups attached to the sulfonate moieties. The resilience of the GS network simplifies crystal design and synthesis by constraining the crystal packing in two dimensions so that the remaining third dimension can be engineered reliably through the introduction of interchangeable organic groups. The guanidinium organomonosulfonates (GMS) assemble through interdigitation of the sulfonate organic groups that project from the surfaces of the GS sheets,[14−18] commonly forming either a bilayer or simple continuously layered (s-CL) architecture,[19] depending on the cross-sectional area of the organic group (Figure 2A,B). Guanidinium organodisulfonates

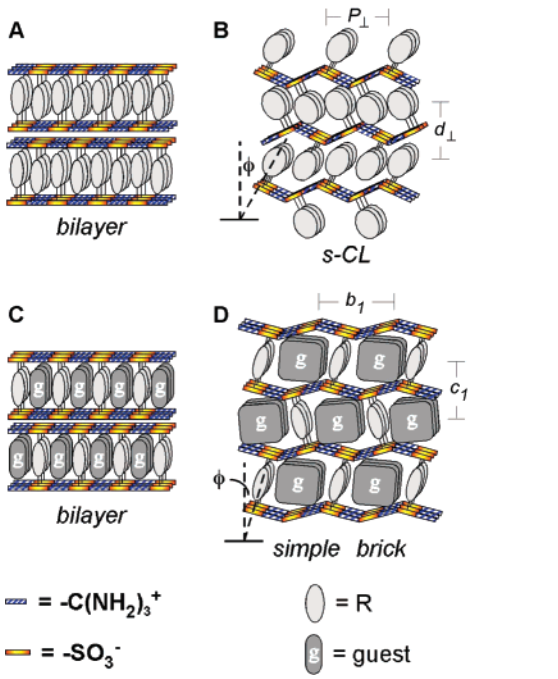

Figure 2. Schematic representations of (A) guest-free GMS bilayer architecture, (B) guest-free GMS simple continuously layered (s-CL) architecture, (C) GDS inclusion compound with the discrete bilayer architecture, and (D) GDS inclusion compound with the simple brick architecture. The organic groups in the GMS s-CL and GDS simple brick frameworks have identical "up−down" projection topologies on each GS sheet (see Figure 5).

(GDS) assemble via organodisulfonate "pillars" that connect opposing GS sheets, thus enforcing inclusion cavities in the gallery regions between adjacent GS sheets (Figure 2C,D).[20] GDS compounds have been found to exhibit numerous framework architectures—discrete bilayer, simple brick, double brick, zigzag brick, V-brick—as a consequence of templating by the guests during assembly of the crystal lattice.[21−23]

The GS sheet has been observed for a wide range of organic substituents in GMS compounds and numerous pillar-guest combinations in GDS compounds. Its extraordinary persistence can be attributed to (i) the ionic character of the N−H···O−S hydrogen bonding, (ii) an inherent structural compliance of the GS sheet (through puckering), (iii) the availability of an alternative "shifted ribbon" motif in which GS ribbons are joined by only a single N−H···O−S hydrogen bond between the cations and anions, and (iv) access to multiple architectural isomers, the last three features permitting efficient packing of a variety of organic components.[24] In the case of GDS inclusion compounds, the reliability of the GS sheet as a supramolecular building block has permitted systematic modification of the host frameworks, enabling control of crystal symmetry, lattice metrics, and the design of functional materials.[25−28]

A preliminary study in our laboratory revealed the unexpected formation of GMS inclusion compounds, even though inclusion

(6) MacDonald, J. C.; Dorrestein, P. C.; Pilley, M. M.; Foote, M. M.; Lundburg, J. L.; Henning, R. W.; Schultz, A. J.; Manson, J. L. *J. Am. Chem. Soc.* **2000**, *122*, 11692.
(7) Paraschiv, C.; Ferlay, S.; Hosseini, M. W.; Bulach V.; Planeix, J.-M. *Chem. Commun*. **2004**, 2270.
(8) Ferlay S.; Hosseini, M. W. *Chem. Commun*. **2004**, 788.
(9) Palacin, S.; Chin, D. N.; Simanek, E. E.; MacDonald, J. C.; Whitesides, G. M.; McBride, M. T.; Palmore, G. T. R. *J. Am. Chem. Soc*. **1997**, *119*, 11807.
(10) Aakeroy, Christer B.; Beatty, Alicia M.; Leinen, Destin S. *CrystEngComm* **2000**, 145.
(11) Zaworotko, M. J. *Chem. Commun*. **2001**, 1.
(12) Hoffart, D. J.; Dalrymple, S. A.; Shimizu, G. K. H. *Inorg. Chem*. **2005**, *44*, 8868.
(13) Wang, X.-Y.; Justice, R.; Sevov, S. C. *Inorg. Chem.* **2007**, *46*, 4626.
(14) Russell, V. A.; Etter, M. C.; Ward, M. D. *J. Am. Chem. Soc.* **1994**, *116*, 1941−1952.
(15) Russell, V. A.; Etter, M. C.; Ward, M. D. *Chem. Mater*. **1994**, *6*, 1206−1217.
(16) Burke, N. J.; Burrows, A. D.; Mahon, M. F.; Teat, S. J. *CrystEngComm* **2004**, *6*, 429.
(17) Burrows, A. D.; Harrington, R. W.; Mahon, M. F.; Teat, S. J. *Eur. J. Inorg. Chem*. **2003**, 1433.
(18) Kathó, A.; Bényei, A. C.; Joó, F.; Sági, M. *Adv. Synth. Catal*. **2002**, *344*, 278.
(19) The s-CL architecture previously was denoted only as CL because no other architecture had yet been discovered. The discovery of the new architectures described herein, however, demand a more definitive nomenclature.
(20) Russell, V. A.; Evans, C. C.; Li, W.; Ward, M. D. *Science*, **1997**, *276*, 575−579.
(21) Swift, J. A.; Pivovar, A. M.; Reynolds, A. M. *J. Am. Chem. Soc*. **1998**, *24*, 5887.
(22) Swift, J. A.; Reynolds A. M.; Ward, M. D. *Chem. Mater*. **1998**, *10*, 4159.
(23) Holman, K. T.; Martin, S. M.; Parker, D. P.; Ward, M. D. *J. Am. Chem. Soc.* **2001**, *123*, 4421.
(24) Architectural isomerism is a term used to describe framework isomers having identical composition and supramolecular connectivity (e.g., the H-bonded GS sheet) but different connectivity patterns in the third dimension owing to the different up−down configurations.

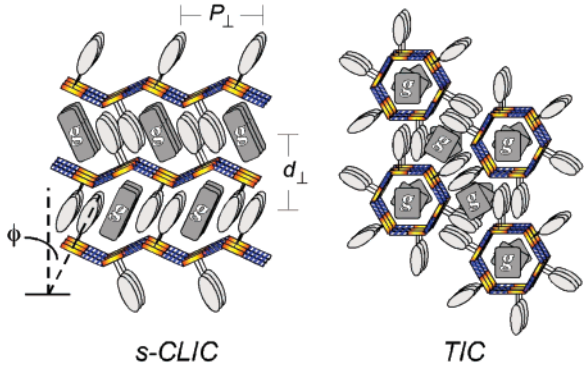

Figure 3. Schematic representations of the GMS s-CLIC and TIC architectures. Guest molecules (g) are included in the framework cavities. The TICs contain guest molecules within and between the cylinders.

cavities in these compounds are not predestined, as they are in the GDS frameworks. Certain GMS−guest combinations generated a lamellar architecture, denoted as a simple continuously layered inclusion compound (s-CLIC),[29] in which the organomonosulfonates adopted a projection topology identical to that of the guest-free s-CL compounds but with guests confined between the organic groups of the organomonosulfonates (Figure 3A).[30] The GS sheets in these inclusion compounds can be viewed as "molecular jaws" in which organomonosulfonate groups projecting from opposing sheets close around the guest molecules. Surprisingly, some host−guest combinations generated tubular inclusion compounds (TICs) in which guest-filled cylinders, constructed from the quasihexagonal GS motif, organized into hexagonal arrays through interdigitation of the organic groups projecting from the outer surface of each cylinder (Figure 3B). This behavior contrasts with GDS inclusion compounds, which can form only lamellar structures. Furthermore, the TICs crystallized in hexagonal space groups, which are rare among molecular crystals. This lamellae-cylinder isomerism, which results from curvature of the elastic GS sheet with retention of its supramolecular connectivity, is unusual for molecular crystals, resembling more the structural isomerism often associated with "soft matter" surfactant assemblies and block copolymers.[31−35]

The persistence of the GS network for different organosulfonates offers a rare opportunity for comprehensive and systematic examination of the relationship between framework architectures and the molecular components. We describe herein GMS inclusion compounds, prepared from libraries of 24 benzenesulfonates and 26 guest molecules. Although all of the GMS compounds readily form guest-free phases, 304 inclusion compounds out of a possible 624 were realized, revealing a remarkable capacity of GMS compounds for guest inclusion. In addition to the s-CLIC and TIC forms, these libraries produced several new architectures, some with topologies identical to those observed in the GDS compounds. The host architectures can be grouped into sectors on a "structural phase diagram" on the basis of simple molecular parameters, enabling more reliable

Scheme 1

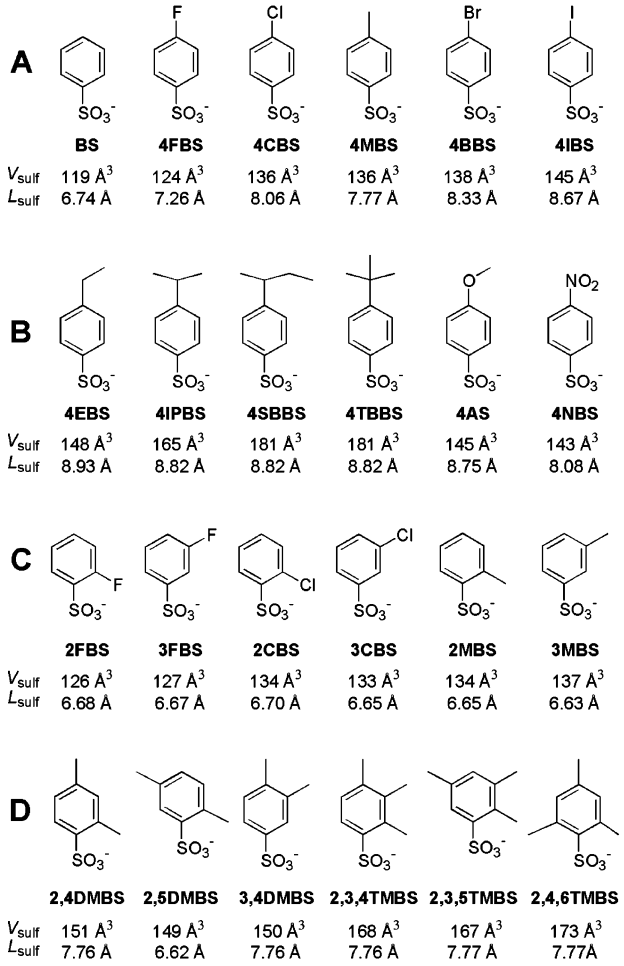

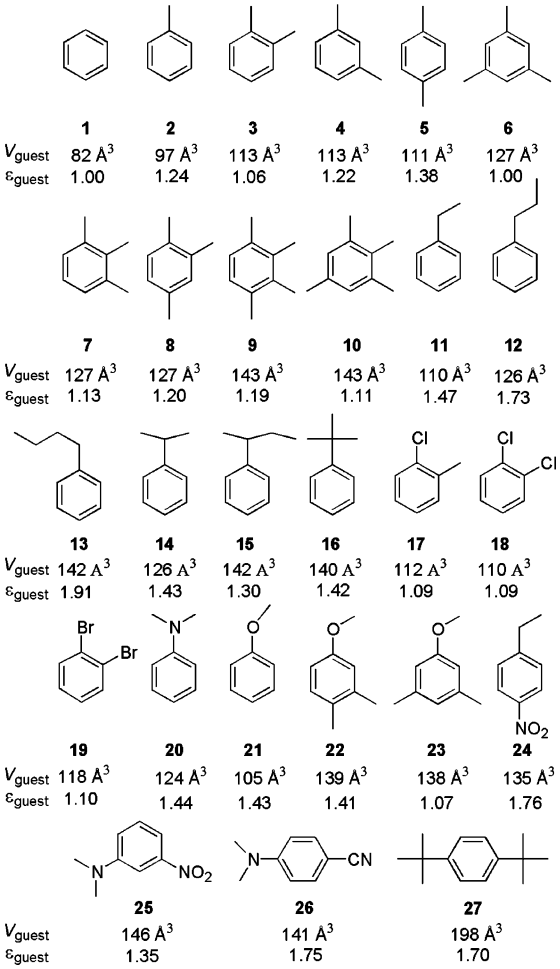

structure prediction for this class of compounds than for molecular crystals in general.

Results and Discussion

Molecular Libraries. Crystalline guest-free GMS compounds and GMS inclusion compounds were prepared from a library of 24 organomonosulfonates, which were chosen to span a range of sizes and shapes (Scheme 1). Crude GMS salts were first prepared by combining acetone solutions of guanidinium tetrafluoroborate and a select organomonosulfonic acid, which produced a crystalline precipitate of the corresponding white or off-white guest-free GMS compound. Single crystals of the guest-free GMS compounds for all 24 organomonosulfonates in Scheme 1 were obtained either by slow cooling or slow evaporation (at room temperature) of saturated methanol solutions. Except for guest-free **G4SBBS**, which formed extremely thin plates that diffracted poorly, these procedures produced crystals suitable for single-crystal X-ray diffraction. GMS inclusion compounds with the general formula GMS•*n*(guest) were prepared either by slow cooling or evaporation of methanol solutions of a particular GMS compound and a guest selected from Scheme 1. Inclusion compounds of guests that were liquids at room temperature (guests **1**−**24**) could be grown at the interface between the liquid guest and a methanol solution of a GMS salt. Guest **27**, 1,4-di-*tert*-butylbenzene, is included in Scheme 1 even though its inclusion was examined only with respect to **G4TBBS•(27)**, which was discovered during attempts to prepare guest-free **G4TBBS** (**27** was a minor impurity in **4TBBS** owing to its presence in the *tert*-butylbenzene starting material). The combination of the 24 organomonosulfonates and 26 arene guests in Scheme 1 (i.e., excluding guest **27**) corresponds to 624 unique host−guest combinations.

Guest-Free GMS Compounds. Guest-free GMS compounds previously reported by our laboratory (44 total) crystallized predominantly in layered structures—the bilayer and s-CL architectures—enforced by the GS sheet (39 of 44).[14,15] Organomonosulfonate substituents with larger cross-sectional areas favored formation of the s-CL architecture, which creates more area on the GS sheet, compared with the bilayer, enabling interdigitation of larger organic groups. The 15 new structures determined here (Supporting Information, Table S1) reinforce the role of the size and shape of the organomonosulfonate group in crystal architecture. For convenience, the description of the structures of these guest-free compounds, as well as nine previously reported ones, have been grouped into four categories according to the number, position, and size of substituents attached to the arene ring of the organomonosulfonate: (*A*) H, F, CH_3, Cl, Br, I substituents on the para position; (*B*) bulky substituents (ethyl, isopropyl, *sec*-butyl, *tert*-butyl, methoxy, nitro) on the para position; (*C*) CH_3, F, and Cl on the ortho and meta positions; (*D*) multiple methyl substituents. This grouping also is used later for the corresponding inclusion compounds (crystallographic details reported in Table S1 pertain to new guest-free GMS compounds only).

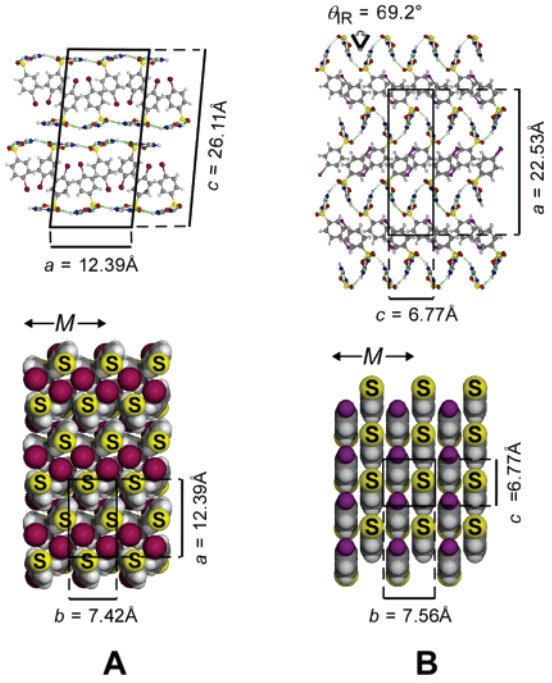

Figure 4. (A) Guest-free GMS bilayer **G4BBS** (**PT-I**) and (B) s-CL **G4IBS** (**PT-II**) as viewed down the GS ribbon axes (top) and perpendicular to the GS sheets (bottom). The G ions and S oxygen atoms in the GS sheets have been removed in the bottom panels to reveal the packing of the organic groups. M denotes the major ribbon direction.

Group A: Para-Substituted Benzenesulfonates. Guest-free **GBS**, **G4CBS**, **G4MBS**, and **G4BBS** crystallized in the bilayer architecture with the quasihexagonal GS sheet, as depicted here for **G4BBS** (Figure 4; a summary of key structural features for the guest-free GMS compounds is included in Table 1). Using a classification scheme described for organodisulfonate pillars in GDS compounds,[23] the quasihexagonal GS sheet can be described as consisting of one "major" (*M*) and two "minor" (*m*) ribbons, and the "up−down" projections of the organomonosulfonate groups from the two sides of the GS sheet can be represented on a "projection topology" diagram as filled or open circles (Figure 5; up = filled circles, down = open circles). Because the GS sheet is infinite in two dimensions, the number of possible "up−down" arrangements of organosulfonate groups is indefinite. The bilayer architecture has a projection topology (PT) in which the organic groups on each sheet project from the same side; thus, all the sulfonate nodes are decorated with filled circles (**PT-I**).

(25) Holman, K. T.; Pivovar, A. M.; Swift, J. A.; Ward, M. D. *Acc. Chem. Res.* **2001**, *34*, 107.
(26) Although the GS sheet has proven remarkably robust, it can be disrupted by strong hydrogen-bonding substituents on the organomonosulfonate or organodisulfonate components that compete for the (guanidinium)N-H and sulfonate(S-O) binding sites, see: Russell, V. A.; Etter, M. C.; Ward, M. D. *Chem. Mater.* **1994**, *6*, 1206. Consequently, components of this type generally are avoided. Although rare, the quasihexagonal GS motif also can be disrupted by large numbers of dispersive contacts between the organic components, as observed in G·SO_3-(C_6H_4)(CH_2)$_{13}CH_3$), for which alkyl−alkyl packing requirements compete with the hydrogen bonds of the quasihexagonal sheet, see: Martin, S. M.; Yonezawa, J.; Horner, M. J.; Macosko, C. W.; Ward, M. D. *Chem. Mater.* **2004**, *16*, 3045.
(27) Pivovar, A. M.; Holman, K. T.; Ward, M. D. *Chem. Mater.* **2001**, *13*, 3018.
(28) Holman, K. T.; Pivovar, A. M.; Ward, M. D. *Science* **2001**, *294*, 1907.
(29) The s-CLIC architecture previously was denoted as simply CLIC in ref 41 because no other lamellar architecture for GMS inclusion compounds had yet been discovered. The discovery of the new architectures described herein demands a more definitive nomenclature.
(30) Horner, M. J.; Holman, K. T.; Ward, M. D. *Angew. Chem., Int. Ed.* **2001**, *40*, 4045.
(31) Whitten, T. A.; Pincus, P. A., *Structured Fluids: Polymers, Colloids, Surfactants*; Oxford University Press: Oxford, England, 2004.
(32) Seddon, J. M.; Hogan, J. L.; Warrender, N. A.; Pebay-Peyroula, E. *Prog. Colloid Polym. Sci.* **1990**, *81*, 189.
(33) (a) Luzzati, V. In *Biological Membranes*; Chapman, D., Ed.; Academic Press: London, 1968; Vol. 1, pp 71−123. (b) *Biochim. Biophys. Acta* **1990**, *1031*, 1.
(34) Matsen, M. W.; Bates, F. S. *J. Chem. Phys.* **1997**, *106*, 2436.
(35) Bates F. S.; Frederickson, G. H. *Phys. Today* **1999**, *52* (2), 32.

Table 1. Selected Structural Features for GMS Guest-free Compounds Exhibiting the Bilayer (BL), Opposed Cylinder (LC), Simple Continuously Layered (s-CL), Double Bilayer (DL), and Double Continuously Layered (d-CL) Architectures

compound[a]	space group	L_{sulf}[b] (Å)	V_{sulf}[c] (Å^3)	V_{host}[c] (Å^3)	architecture	$d_\perp$[d] (Å)	ring offset[e] (Å)	arene packing[f]	arene–arene dihedral angle[g]	V_{cell}[c] (Å^3)	θ_{IR}	PF
					Group A							
GBS	$P2_1/c$	6.74	118	168	BL	11.64	0.14	HB	54.4°	263	169.7°	0.67
G4FBS	$P2_1/c$	7.26	124	174	LC	NA[h]	0.2, 0.4	HB	58.0°, 35.0°	268	176.2°	0.65
G4CBS	$P2_1/c$	8.06	136	186	BL	12.72	1.0, 1.7	HB	56.2°, 70.4°	292	173.7°	0.64
G4MBS	$P2_1/c$	8.06	136	186	BL	12.80	1.2, 1.7	HB	50.3°, 71.0°	295	174.2°	0.64
G4BBS	$P2_1/c$	8.33	140	190	BL	13.00	1.6, 2.1	HB	55.0°, 73.2°	299	175.1°	0.64
G4IBS	*Pnma*	8.67	141	191	s−CL	11.26	1.1	HB	0°[l]	288	69.2°	0.66
					Group B							
G4EBS	*Ama2*	8.93	147	197	s−CL(p)[l]	10.92	1.4	FTF	0°	293	72.7°	0.67
G4IPBS	*Pbca*	8.82	166	216	DBL	23.79	2.7	HB	81.0°, 81.6°	365	180°	0.59
G4TBBS	*Pbca*	8.82	182	232	zz−CL(A)	11.06	1.7	HB	NA[j]	335	180°	0.69
G4AS	$P2_1/c$	8.75	145	195	BL	13.75	1.7, 2.6	HB	70.7°, 72.2°	310	172.9°	0.63
G4NBS	*Ama2*	8.08	146	196	s−CL(p)[l]	10.35	1.0	FTF	0°	284	75.0°	0.69
G4NBS	$P2_1/c$	8.08	146	196	disrupted	10.51	1.4	HB	72.5°	267	NA[k]	0.73
					Group C							
G2FBS	$C2/c$	6.68	125	175	BL	10.60	0.8	FTF	0°	269	180°	0.65
G3FBS	$P\bar{1}$	6.67	126	176	BL	10.97	0.4	FTF	0°	256	180°	0.69
G2CBS	$P\bar{1}$	6.70	133	183	BL	11.48	0.7	FTF	0°	270	180°	0.68
G3CBS	$P\bar{1}$	6.65	132	182	BL	11.57	1.0	FTF	0°	274	180°	0.67
G2MBS	*Pnma*	6.65	134	184	s-CL	8.16	1.1	FTF	0°	284	103.0°	0.65
G3MBS	*Pnma*	6.63	132	182	s-CL	8.71	1.3	FTF	0°	285	92.2°	0.64
					Group D							
G2,4DMBS	$Pmc2_1$	7.76	152	202	d-CL	12.06	1.5	FTF	0°	313	70.2°, 141.4°	0.64
G2,5DMBS	*Pnma*	6.62	151	201	s-CL	8.31	1.0	FTF	0°	297	104.0°	0.68
G3,4DMBS	*Pnma*	7.76	151	201	s-CL	9.35	1.8	FTF	0°	295	72.7°	0.70
G2,3,4TMBS	*Pnma*	7.76	166	216	s-CL	10.02	2.6	FTF	0°	323	91.8°	0.67
G2,4,5TMBS	*Pnma*	7.77	167	217	s-CL	9.26	2.0	FTF	0°	326	101.0°	0.67
G2,4,6TMBS	*Pnma*	7.77	172	222	s-CL	10.46	1.9	FTF	0°	333	83.6°	0.66

[a] Compounds in italics have been reported previously. [b] L_{sulf} represents the length of the organomonosulfonates as measured from the center of the sulfur atom to the most distant atom, accounting for its van der Waals radius of the distant atom. [c] V_{sulf} represents the molecular volume of the organomonosulfonates as calculated with Connolly surfaces in the Cerius^2 environment. V_{host} represents the sum of V_{sulf} and the volume of the guanidinium ion. V_{cell} correspond to one **GS** formula unit. [d] $d_\perp$ is calculated as one-half of the unit cell constant in the direction normal to the GS sheet, which represents the lamella thickness in the bilayer architecture and the interplaner GS sheet distance in the remaining architectures. [e] Lateral offset of arene rings projecting from opposing GS sheets (see Figure 5). Entries with two values signify two crystallographically unique pairs of arene rings projecting from opposing sheets. In the case of **G4FBS**, the first entry corresponds to the offset of the arene rings inside the cylinder and the second to the offset of arene rings between the cylinders. [f] FTF = face-to-face, HB = herringbone. [g] Angle measured between mean planes of adjacent arene groups on adjacent organomonosulfonates. [h] The value of $d_\perp$ for **G4FBS** is not applicable because the GS sheet is not lamellar. [i] The arene rings were modeled as face-to-face in the structure solution; however, there was sufficient electron density, out of the plane of the arene ring, to indicate slight herringbone character. [j] The arene−arene dihedral angle for **G4TBBS** is not applicable because the bulky isopropyl group prevents close packing of adjacent rings. [k] q_{IR} is not applicable because the GS sheet is discontinuous. [l] s-CL(p) denotes simple continuously layered in a polar space group.

The bilayer topology creates narrow channels on the surface of each sheet that can be filled by organic groups from the opposing sheet, provided the organic groups are sufficiently small to allow interdigitation. In the case of **GBS**, **G4CBS**, **G4MBS**, and **G4BBS**, the aromatic groups on opposing sheets form interdigitated arrays with a herringbone motif (denoted in Table 1 as HB), which is observed in crystals of small arenes.[36] The in-plane lattice constants for these compounds are nearly identical, **GBS** = 7.50, 12.06 Å; **G4CBS** = 7.44, 12.33 Å; **G4MBS** = 7.42, 12.44 Å, and **G4BBS** = 7.42, 12.39 Å, reflecting the structure-enforcing metrics of the GS sheet and the similar footprint areas of the arene rings. The organomonosulfonate arene rings in each of these compounds are tilted somewhat with respect to the direction perpendicular to the sheet, which forces the sulfonate groups to rotate slightly out of the mean plane of the GS sheet. Consequently, the metrics of a strictly planar GS sheet appear to be slightly incompatible with optimum packing of the organic groups but not to the extent that the GS sheet loses its quasihexagonal connectivity.

The lamellar thickness, $d_\perp$, for the bilayer compounds in group A increases monotonically with increasing organomonosulfonate length (L_{sulf}, as measured from the sulfur atom to the para substituent, including its van der Waals radius; Table 1). Because of steric interactions between the para substituents and the opposing GS sheet, an increase in L_{sulf} is necessarily accompanied by an increasing offset (Figure 6) of the interdigitated arene rings in the order **GBS** = 0.14 Å < **G4CBS** = 1.0, 1.7 Å < **G4MBS** = 1.2, 1.7 Å < **G4BBS** = 1.6, 2.1 Å (pairs of values reflect crystallographically unique pairs of arene rings).

An increase in the arene offset, which reduces the intermolecular overlap between the arene rings on opposing GS sheets, would be expected to reduce the stability of the interdigitated bilayer. This offset apparently reaches a stability limit for **4IBS**, as **G4IBS** adopts the s-CL architecture (**PT-II**) rather than a more expanded bilayer. The GS sheets in **G4IBS** are highly puckered, which permits 4IB rings on opposing sheets in **G4IBS** to achieve a ring offset of 1.1 Å.[37] This value is comparable to those observed for the **G4MBS** and **G4CBS** bilayer structures, suggesting recovery of the cohesive intermolecular forces required for crystallization. The accordion-like puckering is

(36) Gavezotti, A.; Desiraju, G. R. *J. Chem. Soc., Chem. Comm.* **1989**, 621.

(37) Although the structure solution portrays adjacent iodobenzene rings as coplanar, the large isothermal parameters of the arene carbons suggest that the arene groups are slightly disordered on two positions indicating a degree of herringbone character between organic groups from opposing GS sheets.

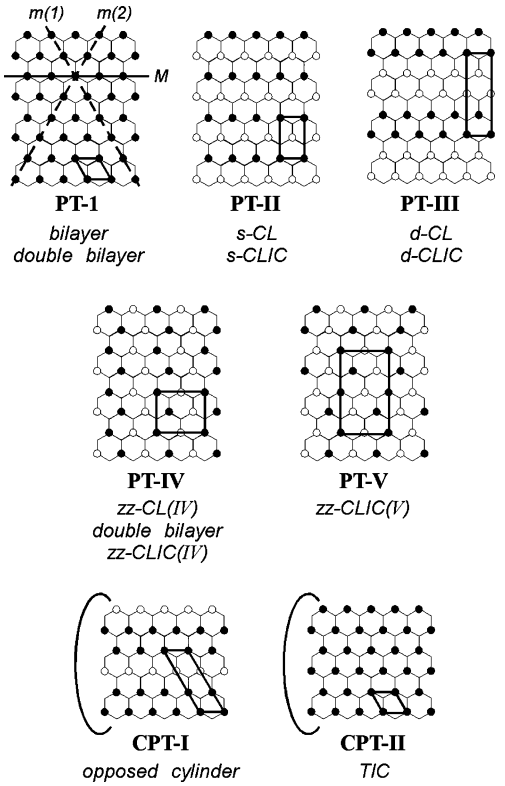

Figure 5. Projection topologies (PT) for GS sheets observed in the guest-free and guest-inclusion architectures. The projected topologies are denoted by Roman numerals, and architectures containing these topologies are listed below each example. Filled and open circles depict organic groups projecting from the sulfonate nodes above and below the sheet, respectively. The G ions sit on the undecorated nodes of the hexagonal tiling. **PT-I** illustrates the major ribbon (*M*) and minor ribbons, *m*(1) and *m*(2). The parallelograms depict the translational repeat unit of each sheet. The loops sketched on the cylindrical projection topologies (**CPT-I** and **CPT-II**) denote hydrogen-bonded fusion of the edges of the GS ribbons at the top and bottom of each diagram, which results in formation of cylinders enclosed by a continuous guanidinium−sulfonate network. Key for acronyms: s-CL = simple continuous layered; s-CLIC = simple continuous layered inclusion compound; d-CL = double continuous layered; d-CLIC = double continuous layered inclusion compound; zz-CL = zigzag continuous layered; zz-CLIC = zigzag continuous layered inclusion compound (two versions); TIC = tubular inclusion compound.

substantial (θ_{IR} = 69°), reflecting the small volume of the iodobenzene group compared with the amount of free volume available in a hypothetical unpuckered s-CL architecture, which can be discerned from a comparison of the bilayer s-CL projection topology diagrams. Puckering reduces the free volume and allows denser packing of the organic groups. In the case of **G4IBS**, the 4IB groups are canted along the direction perpendicular to the major ribbons (that is, perpendicular to the pleats of the accordion), producing edge-to-edge contacts between adjacent 4IB groups that create channels on the GS sheet. These channels become occupied by the 4IB groups from the opposing sheet.

Guest-free **G4FBS** adopts a unique and unexpected architecture consisting of layers of discrete rhomboid cylinders (Figure 7). Each cylinder consists of six GS ribbons fused edge-to-edge, closing to form a continuous surface with the quasi-hexagonal motif, that is, the same hydrogen-bond connectivity observed in the GMS bilayer and s-CL architectures. The $d_{N\cdots O}$ hydrogen-bond distances connecting the corners at the acute ends of the rhomboid are slightly longer than the typical values for the quasihexagonal GS sheet ($d_{N\cdots O}$ = 3.044 and 3.112 Å vs 2.90 Å), but still within acceptable limits for hydrogen bonding. The internal volume of the cylinders is occupied by one-third of the fluorobenzene groups. The remaining 4FB groups projected outward from the cylinders, which assemble into layers by interdigitation. Consequently, the projection topology of **G4FBS** is **CPT-I** in Figure 5 (C denotes cylinder, in order to distinguish the topology from the lamellar forms). The structural characterization of numerous GS compounds has revealed that the spacing between sulfonate groups along the GS ribbon is effectively immutable, with an average value of $d_{S\cdots S}$ = 7.5 ± 0.2 Å, ideal for interdigitation of groups from opposing ribbons. Indeed, the respective distances between the centroids of the intracylinder and intercylinder fluorobenzene rings in **G4FBS** is 3.72 Å, effectively equivalent to $d_{S\cdots S}/2$ (ca. 3.75 Å). Consequently, $d_{S\cdots S}$ imposes an upper limit on the number of fluorobenzene rings that can project into the cylinder (the open circles in the topology diagram in Figure 5). Moreover, because the GS cylinder contains an even number of ribbons, the fluorobenzene groups on the two opposing ribbons naturally are shifted by $d_{S\cdots S}/2$, producing the registry required for interdigitation. The asymmetric projection topology of the cylinders—two 4FB rings inward and four outward—results in a rhomboid morphology instead of the perfectly cylindrical morphology observed for the TIC architecture (see below).

Group B: Benzenesulfonates with Bulky Para Substituents. Guest-free GMS compounds with benzenesulfonates having bulky para substituents adopted architectures unlike those observed for the compounds in group A. Previous work in our laboratory[38,39] revealed a polar s-CL architecture (**PT-II**) for **G4EBS** and α-**G4NBS**, both crystallizing in space group *Ama*2,[40] resembling the orthorhombic polar frameworks observed for GDS inclusion compounds with "banana-shaped" pillars.[41] The GS sheets in **G4EBS** and α-**G4NBS** adopt the quasihexagonal motif and are highly puckered (θ_{IR} = 72.7° and 75.0°, respectively; Figure 8). The organic groups from adjacent layers are stacked face-to-face (denoted FTF in Table 1) with centroid-to-centroid distances of 3.72 Å, as prescribed by the intraribbon $d_{S\cdots S}/2$ value. As a consequence of the puckering, the long axes of the 4EB and 4NB groups are oriented along the polar *c*-axis, forming angles of 46.8° and 47.3° with respect to the *c* axes. The ethyl groups in **G4EBS** are directed toward the V-shaped nook of the puckered GS sheet and one oxygen atom on each of the nitro groups in **G4NBS** forms a weak hydrogen-bonding contact with the guanidinium cations (Figure 8).

Guest-free **G4IPBS** adopted a new architecture, a "double bilayer", which contained structural features of both the discrete

(38) Martin, S. M.; Yonezawa, J.; Horner, M. J.; Macosko, C. W.; Ward, M. D. *Chem. Mater.* **2004**, *16*, 3045.
(39) Russell, V. A.; Etter, M. C.; Ward, M. D. *Chem. Mater.* **1994**, *6*, 1206.
(40) During the course of these studies, a second polymorph of **G4NBS** was discovered, hereafter denoted as β-**G4NBS** that crystallized in the centrosymmetric $P2_1/c$ space group. The guanidinium ions and sulfonate moieties in β-**G4NBS** adopt an uncharacteristic motif in which the strongest hydrogen bonds between guanidinium ions and the sulfonate moieties ($d_{N-H\cdots O}$ < 2.1 Å) wind about the *a* axis like a helix, effectively forming bridges between opposing rows of **4NBS** molecules. Inspection of the crystal structure also reveals short contacts between the nitro oxygen atoms and the guanidinium nitrogen atoms (3.04 Å), which interfere with the formation of the quasihexagaonal hydrogen-bonding motif and compensate for the subsequent loss of some of the N−H···O(sulfonate) hydrogen bonds. The arene rings on adjacent assemblies interdigitate through edge-to-face interactions, resulting in formation of a layered architecture. The arene offset value for β-**G4NBS** is slightly larger (1.5 Å) than that of α-**G4NBS** (1.0 Å), but within the range observed for the guest-free GMS compounds.
(41) Holman, K. T.; Pivovar, A. M.; Ward, M. D. *Science* **2001**, *294*, 1907.

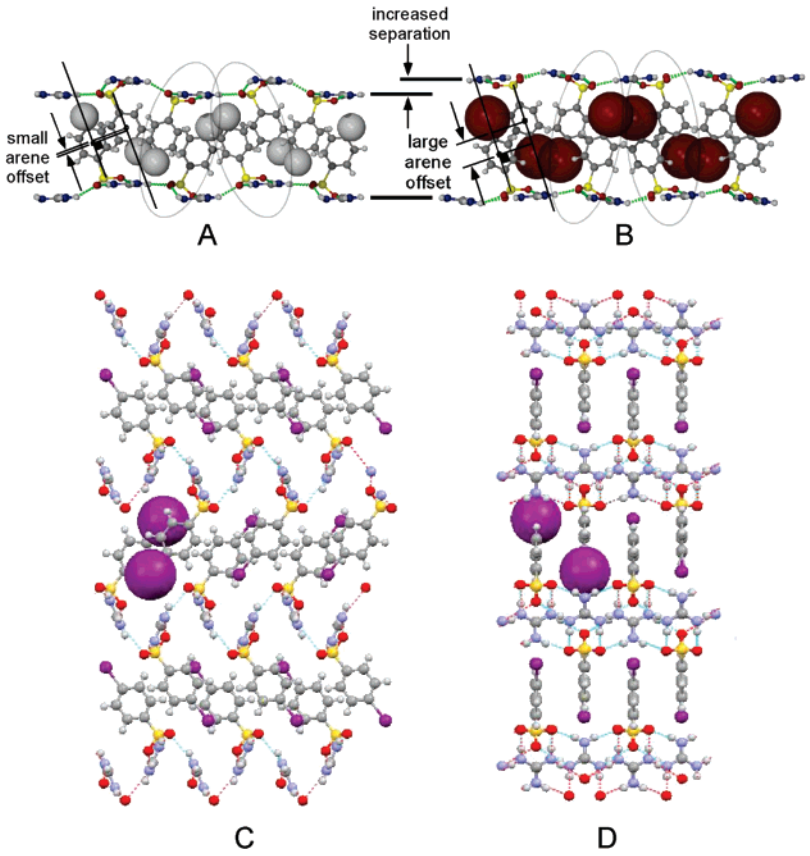

Figure 6. Increasing the size of para substituents, rendered as van der Waals spheres for (A) **GBS** and (B) **G4BBS**, increases the separation between opposing GS sheets for guanidinium para-substituted benzenesulfonates. The crystal structure of the s-CL architecture in **G4IBS**, as viewed normal to the (C) *ab* and (D) *ac* planes. Dense packing of the *p*-iodobenzene groups is achieved through puckering of the **GS** sheets, which maintain their quasihexagonal connectivity. Two of the iodine substituents are rendered as van der Waals spheres. The puckering allows the *p*-iodobenzene groups to recover a 1.1 Å ring offset, which is typical of the bilayer compounds.

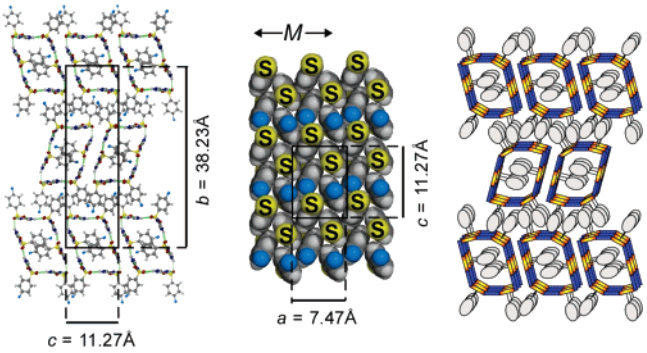

Figure 7. Guest-free **G4FBS**, which adopts an opposed-cylinder architecture (projection toplogy cylinder I). The left panel depicts the view along the GS ribbons. The center panel depicts the view perpendicular to the GS sheets, where the G ions and S oxygen atoms in the GS sheets have been removed to reveal the packing of the organic groups. The right panel is a schematic representation of the **G4FBS** compound. *M* denotes the major ribbon direction.

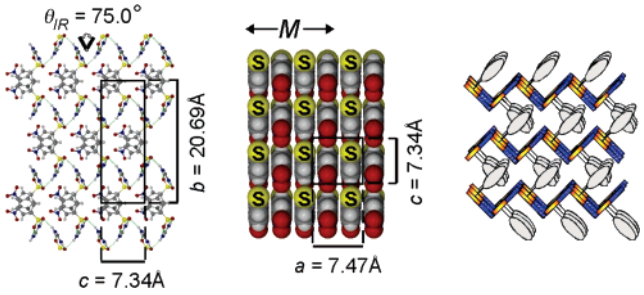

Figure 8. Guest-free α-**G4NBS**, which adopts a polar s-CL architecture (**PT-II**). The center panel depicts a view perpendicular to the GS sheets, where the G ions and S oxygen atoms in the GS sheets have been removed to reveal the packing of the organic groups. The right panel is a schematic representation of the compound. *M* denotes the major ribbon direction.

bilayer and s-CL architectures (Figure 9). Although this is the only example to date of a mixed topology in a single GMS compound, the same topology was reported recently for $[C(NH_2)_2(NHMe)][1\text{-naphthalenesulfonate}]$.[42] The two outer sheets in **G4IPBS** exhibit the **PT-I** bilayer topology, with all of the 4IPB groups projecting toward the interior. The 4IPB groups on the center GS sheet form zigzag channels with topology **PT-IV**, generating an architecture identical to that observed in zz-CL(IV) compounds. Because only one-half of the organic groups project from each side of the center sheet, the zigzag channels can accommodate *two* outer-sheet 4IPB groups for each IPB group on the center sheet. The **PT-IV** topology is an "egg-carton-like" puckering of the GS sheet instead of the accordion-like puckering observed in the s-CL architecture (**PT-II**); the latter is allowed only if the organic substituents project from the same side along a major ribbon.

Guest-free **G4TBBS** adopted yet another new architecture in which hydrogen-bonded quasihexagonal GS "rafts" stacked continuously along the *b*-axis through interdigitation of the bulky 4TBB groups projection from opposing sheets, which adopted

(42) Burke, N. J.; Burrows, A. D.; Mahon, M. F.; Warren, J. E. *CrystEngComm* **2006**, *8*, 931.

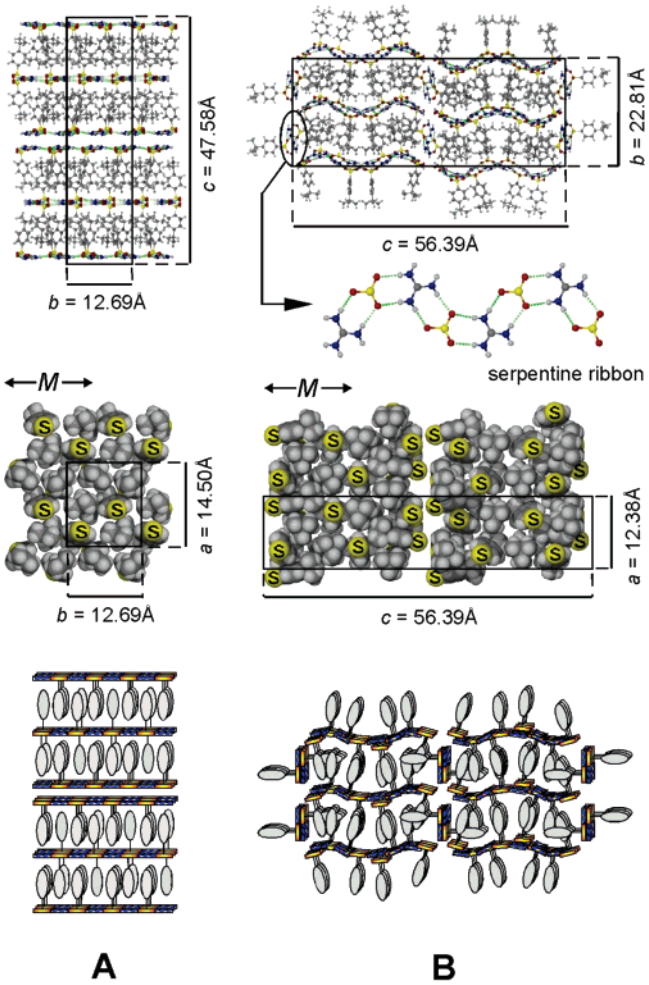

Figure 9. Guest-free GMS compounds: (A) **G4IPBS**, which exhibits the double bilayer (DBL) architecture in which the top and bottom sheets adopt **PT-I** and the inner sheets adopt topology **IV**. (B) **G4TBBS**, which adopts a ladderlike architecture in which rafts having the zigzag **PT-IV** stack continuously but are truncated by serpentine ribbons that span the gallery separating the rafts. The center panels depict views perpendicular to the GS sheets, where the G ions and S oxygen atoms in the GS sheets have been removed to reveal the packing of the organic groups. In the case of the **G4IPBS**, the perpendicular view depicted corresponds to the sheet in the center of the double bilayer. *M* denotes the major ribbon direction. The bottom panels are schematic representations.

PT-IV (Figure 9B). The edges of the rafts are truncated serpentine GS ribbons that coincide with the *a*-axis and span the thickness of the gallery region, generating a ladderlike architecture. Water molecules bridge the edges of the raft and the serpentine ribbon through linear (ribbon)S−O···H(water) O···H−N(raft) hydrogen bonds (Figure 9). The projection of the 4TBB groups on each serpentine ribbon alternates, up, down, up, down, ..., permitting interdigitation of the 4TBB groups projecting from the GS rafts.

Group C: Ortho- and Meta-Substituted Benzenesulfonates. The halogen-substituted GMS compounds **G2FBS**, **G3FBS**, **G2CBS**, and **G3CBS** adopted bilayer architectures (**PT-I**; Figure 10). **G3FBS**, **G2CBS**, and **G3CBS** are isostructural, all crystallizing in the same space group ($P\bar{1}$) with similar in-plane lattice parameters. The groups projecting from opposing sheets form interdigitated arrays with the arene rings stacked face-to-face, reflecting frustration of the edge-to-face (C−H···π) approach due to the ortho and meta substituents. Surprisingly, **G2FBS**, which crystallized in the monoclinic *C*2/*c* space group, exhibits an ABAB stacking of discrete bilayers; that is, the A and B bilayers are crystallographically distinct. The 2FBS rings from opposing sheets formed interdigitated face-to-face arrays within each bilayer, but the arene rings in bilayer A were rotated by 90° with respect to the arene rings in bilayer B. This unusual ordering between apparently disconnected bilayers signals subtle structure-directing contacts between GS sheets of adjacent bilayers. Despite molecular volumes that are nearly identical with their chloro-substituted homologues, methyl-substituted **G2MBS** and **G3MBS** crystallized in the s-CL architecture (**PT-II**). The GS sheets were highly puckered (θ_{IR} = 103° and 92.2°, respectively), which reflects the small volume of the organic groups relative to the amount of space available in the s-CL lattice. The arene rings from opposing sheets form face-to-face stacks, again reflecting the frustration of edge-to-face ordering by the ortho and meta substituents.

Group D: Multiply Methyl-Substituted Benzenesulfonates. Guest-free **G2,5DMBS**, **G3,4DMBS**, **G2,3,4TMBS**, **G2,4,5TMBS**, and **G2,4,6TMBS** adopted highly puckered s-CL architectures (**PT-II**) with quasi-hexagonal GS sheets, with θ_{IR} ranging from 72.7° for **G3,4DMBS** to 104° for **G2,5DMBS** (Figure 11). The lamellae were assembled by face-to-face stacking of interdigitated arene rings with interplanar spacing of 3.72 Å. In contrast, the **G2,4DMBS** adopted a new architecture, double CL (d-CL), with the **PT-III** topology (Figure 5), identical to that observed in the GDS continuous "double brick" framework.[23] The puckering of the GS sheet in **G2,4DMBS** is more complex than for s-CL forms as it exhibits two distinct puckering angles. This characteristic adds yet another degree of flexibility to the GS sheet so that packing can be optimized for these sterically encumbered organosulfonates. Indeed, the packing fraction for **G2,4DMBS** (PF = 65%) is comparable with all other s-CL structures in this and groups A−C (PF = 67%−68%). The wide ranges of puckering angles and ring offset values for this group (**G2,4DMBS** = 1.5 Å, **G2,5DMBS** = 1.0 Å, **G3,4DMBS** = 1.8 Å, **G2,3,4TMBS** = 2.6 Å, **G2,4,5TMBS** = 2.0 Å, and **G2,4,6TMBS** = 1.9 Å) reflect the different steric demands of the organomonosulfonate groups.

Structural Trends. The discovery of several new lamellar architectures for guest-free GMS compounds, realized by varying the sizes and shapes of the organic groups, reveals the inherent ability of these compounds to optimize packing while retaining the hydrogen-bond connectivity of the quasihexagonal GS sheet and the overall lamellar organization. The persistence the GS sheet, which is uncharacteristic of the organic solid state, can be attributed to several factors: (i) the large number of hydrogen bonds, which are further enforced by the ionic charge of the constituents; (ii) the ability of the 2D sheet to access different projection topologies, which provides a mechanism for accommodating the steric demands of the organic groups; (iii) the compliant character of the GS network, which allows accordion-like puckering in the s-CL and d-CL architectures so that dense packing of the organic constituents can be achieved with retention of the quasi-hexagonal connectivity. This low-energy deformation of the GS network occurs with preservation of the linearity of the N−H···O(sulfonate) hydrogen bonds. If the GS network was rigid, dense packing would not be achievable and it is likely that either crystallization would not occur or that non-lamellar structures with disrupted GS sheets

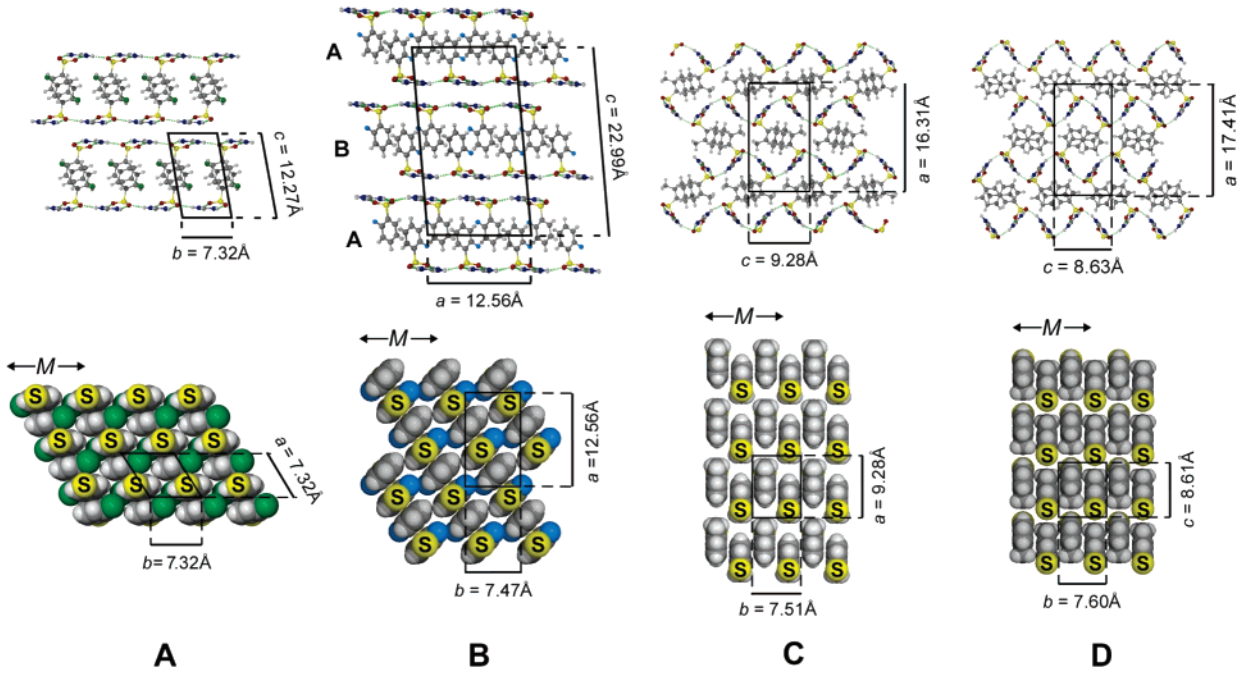

Figure 10. Guest-free GMS compounds with ortho and meta substituents: (A,B) **G2CBS** and **G2FBS**, which both adopt the a bilayer architecture (**PT-I**). **G2FBS**, however, displays an ...ABAB... stacking in which adjacent bilayers are crystallographically distinct. (C,D) **G2MBS** and **G3MBS**, which both adopt the s-CL architecture (**PT-II**). The bottom panels depict views perpendicular to the GS sheets, where the G ions and S oxygen atoms in the GS sheets have been removed to reveal the packing of the organic groups. *M* denotes the major ribbon direction.

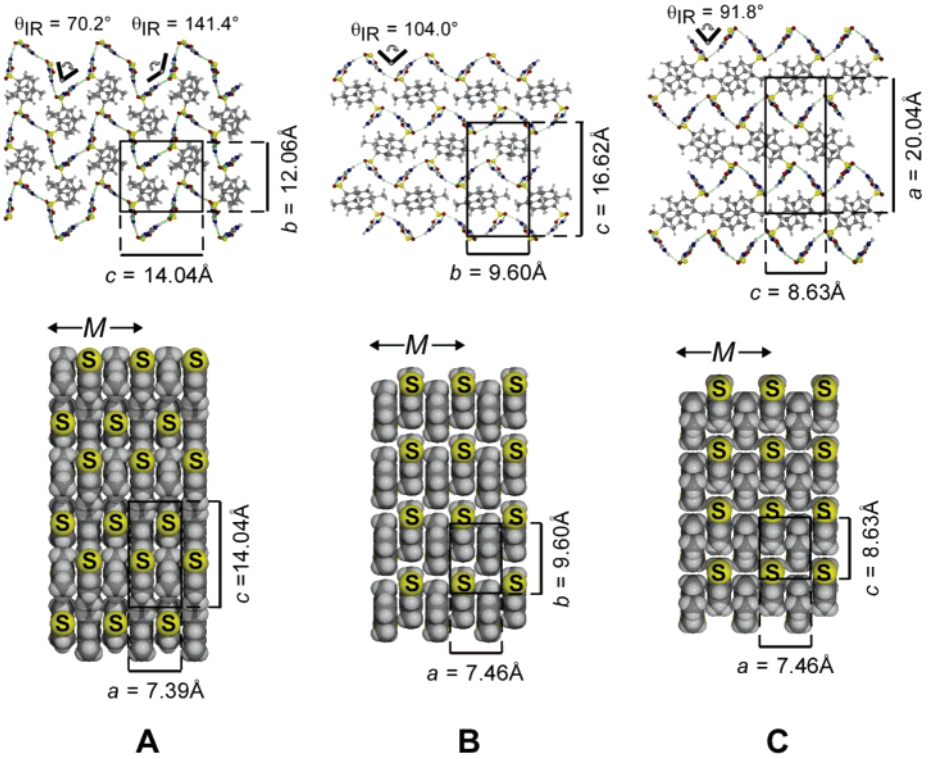

Figure 11. Guest-free GMS compounds with multiple methyl substitutions: (A) Double continuously layered (d-CL) **G2**,**4DMBS**, which adopts projection topology **PT-III**; (B, C) **G2**,**5DMBS** and **G2**,**3**,**4TBBS**, which both adopt the s-CL architecture with the **PT-II** topology. The top panels depict side views along the major ribbon axes. The bottom panels depict views perpendicular to the GS sheets, where the G ions and S oxygen atoms in the GS sheets have been removed to reveal the packing of the organic groups. The interribbon puckering angles (θ_{IR}) are given in the upper panels. *M* denotes the major ribbon direction.

would form. Notably, polymorphism does not appear to be common for guanidinium organosulfonate compounds. With the exception of **G4NBS**, no polymorphs were detected by X-ray powder diffraction for the guest-free compounds derived from the library in Scheme 1.

One consequence of the robustness of the GS frameworks is the emergence of predictable relationships between certain structural parameters, which can be gleaned only when the number of isostructural compounds available is statistically meaningful. We previously demonstrated that the puckering of

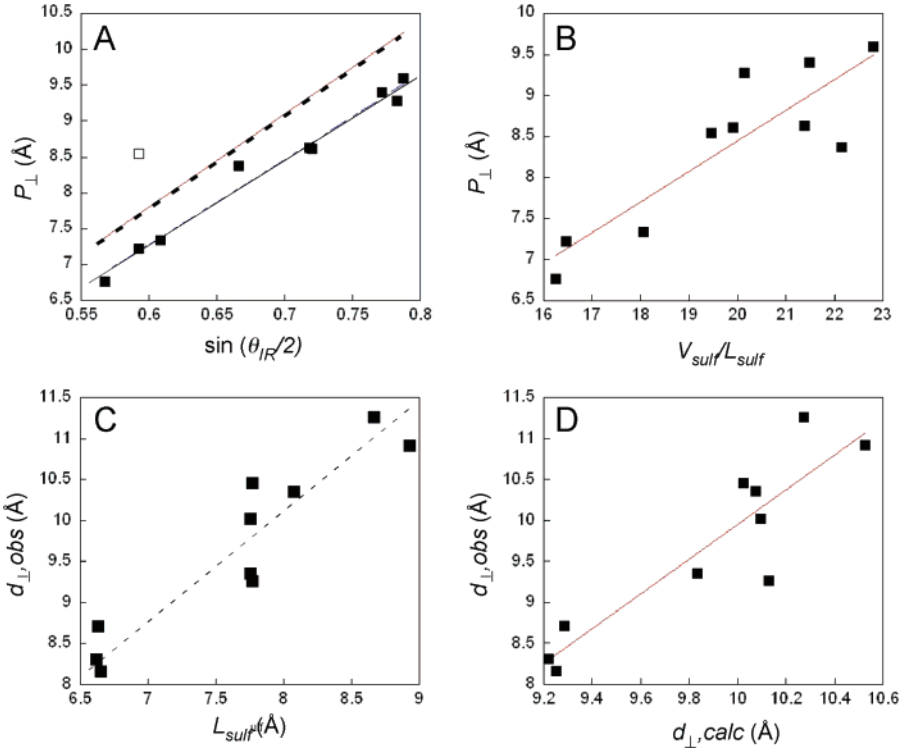

Figure 12. Metric relationships between select structural parameters for guest-free GMS compounds with the s-CL architecture: (A) $P_\perp$ exhibits a linear dependence on sin (θ_{IR}/2), as expected from simple solid geometry. The dashed line represents the ideal dependence based on eq 1. The solid line represents a least-squares fit for the s-CL GMS compounds (the open square, which corresponds to **G3**,**4DMBS**, is not included in the fit). The slope is 12.0 Å, which is slightly less than the value expected from eq 1, and the regression coefficient is $R = 0.99$. The values of $P_\perp$ are approximately 0.5 Å less than the expected value in the region of interest here, but this can be attributed to an effective ribbon width that is smaller than the assumed value of 6.5 Å. (B) The dependence of $P_\perp$ on V_{sulf}/L_{sulf}, which provides an approximation of the "footprint" of the organomonosulfonates on the GS sheet surface. (C) The dependence of $d_{\perp,obs}$ the lattice spacing perpendicular to the GS sheet, on the length of the organomonosulfonates. (D) Comparison of $d_{\perp,obs}$ with the values calculated with eq 2b, assuming $\phi = 90 - \theta_{IR}/2$, which is valid when each organosulfonate is perpendicular to its ribbon.

the GS sheets in the orthorhombic simple brick architecture of guanidinium organo*di*sulfonates was well-behaved, to the extent that b_1, the lattice constant perpendicular to the major ribbons, decreased monotonically with decreasing puckering angle, θ_{IR}, according to the simple algebraic relationship described by eq 1a, in which w is the effective width of a GS ribbon (6.5 Å). Furthermore, the lattice constant perpendicular to the sheets, c_1, conformed to eq 2a, in which l is the length of the organodisulfonate pillar and ϕ its angle of tilt with from a normal to the GS sheet.

Similar trends emerge from the 10 guest-free GMS compounds that crystallize in the s-CL architecture, for which the variables $P_\perp$ (the generic lattice constant perpendicular to the major ribbons), $d_\perp$ (the distance between the centers of adjacent lamellae), and L_{sulf} (the sulfur-to-end length of the organosulfonate) correspond to b_1, c_1, and l in the simple brick architecture, respectively (eqs 1b, 2b). The linear dependence of $P_\perp$ on sin(θ_{IR}/2) (Figure 12A) reveals that the puckering-induced contraction of the lattice along $P_\perp$ is well behaved and occurs without any substantial contributions from other structural distortions.[43] The effect of steric factors is demonstrated further by the monotonic increase of θ_{IR} with increasing values of V_{host}/L_{sulf} (Figure 12B), a quantity that is dimensionally equivalent to the "footprint" of the organosulfonate group on the opposing GS sheet (V_{host} is the combined volume of a particular organomonosulfonate ion and a guanidinium ion; the guanidinium ion has a volume of 50 Å^3). Figure 12C reveals that $d_\perp$ increases with L_{sulf} as expected. Figure 12D displays the comparison between the observed $d_\perp$ values and those calculated using eq 2b, wherein ϕ is not actually measured but is assigned the value $\phi = 90 - \theta_{IR}/2$, which is valid when each organomonosulfonate is perpendicular to its GS ribbon, as is generally the case. Although some scatter exists, the anticipated trend is apparent. One noteworthy feature is the somewhat larger-than-expected observed values of $d_\perp$, which probably can be attributed to inefficient packing of the organic substituents in the pockets of the puckered sheets.

$$b_1 = 2w \sin(\theta_{IR}/2)\ \text{Å} = 13.0 \sin(\theta_{IR}/2)\ \text{Å} \qquad (1a)$$

$$P_\perp = 2w \sin(\theta_{IR}/2)\ \text{Å} = 13.0 \sin(\theta_{IR}/2)\ \text{Å} \qquad (1b)$$

$$c_1 = 13.0 \cos(\theta_{IR}/2) + 2l \cos\phi\ \text{Å} \qquad (2a)$$

$$d_\perp = 6.5 \cos(\theta_{IR}/2) + L_{sulf} \cos\phi\ \text{Å} \qquad (2b)$$

GMS Inclusion Compounds. The facile formation of guest-free GMS compounds for every example in the host library of Scheme 1 would seem to make formation of inclusion compounds unlikely, as GMS compounds are not "predestined" to include guests. Nonetheless, an earlier study in our laboratory

(43) The data reveal a slightly reduced slope (12.0 Å instead of 13.0 Å) and a small reduction of the actual $P_\perp$ values (ca. 0.5 Å) compared with that expected from eq 1b. This minor discrepancy reflects a slight displacement of the sulfur atoms from the ribbon edges. Convenience and accuracy, q_{IR}, is measured using discrete sulfur atoms on adjacent ribbons. Equation 1a and 1b rigorously hold only when θ_{IR} is defined by the intersection of the *mean planes* of two adjacent ribbons.

Table 2. Selected Structural Features of Guest Molecules and GMS Inclusion Compound Architectures for Organomonosulfonates in Group A. (entries shaded in gray represent combinations for which only guest-free GMS compounds crystallized in the presence of the respective guests)

Guest	V_{guest}[b] (Å^3)	L_{guest}[c] (Å)	ε_{guest}[d]	**GBS**	**G4FBS**	**G4MBS**	**G4CBS**	**G4BBS**	**G4IBS**
V_{sulf} (Å^3) / V_{host} (Å^3)[a]				119 / 169	124 / 174	136 / 186	136 / 186	138 / 188	145 / 195
no guest	NA	NA	NA	BL	LC	BL	BL	BL	s-CL
benzene (**1**)	82	6.97	1.00	BL	s-CLIC(||)[e]	BL	s-CLIC	s-CLIC(⊥)[e]	s-CLIC
toluene (**2**)	97	7.98	1.24	BL	s-CLIC	BL	s-CLIC	s-CLIC(⊥)[e]	s-CLIC
anisole (**21**)	105	9.22	1.43	BL	s-CLIC	s-CLIC	s-CLIC	s-CLIC(||)[e]	s-CLIC
ethylbenzene (**11**)	110	9.50	1.47	BL	TIC, s-CLIC	BL	TIC/s-CLIC	TIC	TIC, s-CLIC
1,2-dichlorobenzene (**18**)	110	7.70	1.09	s-CLIC(||)[e]	s-CLIC	s-CLIC	TIC	TIC	s-CLIC
2-chlorotoluene (**17**)	112	7.72	1.09	TIC	s-CLIC	TIC/s-CLIC	TIC	TIC	s-CLIC
o-xylene (**3**)	113	7.44	1.06	TIC,s-CLIC	TIC, s-CLIC	TIC, s-CLIC(||)	TIC	TIC, s-CLIC(⊥)[e]	s-CLIC
m-xylene (**4**)	113	8.65	1.22	s-CLIC	s-CLIC	s-CLIC(||)	s-CLIC(||)[e]	s-CLIC(||)[e]	s-CLIC(||)[e]
p-xylene (**5**)	111	8.89	1.38	s-CLIC(||)[e]	s-CLIC	s-CLIC(||)	s-CLIC(||)[e]	s-CLIC(⊥)[e]	s-CLIC(⊥)[e]
1,2-dibromobenzene (**19**)	118	7.84	1.10	s-CLIC	TIC, s-CLIC	TIC	TIC	TIC	s-CLIC
N,N-dimethylaniline (**20**)	124	9.21	1.44	s-CLIC(||)[e]	s-CLIC(||)[e]	s-CLIC(||)	TIC/s-CLIC	TIC	s-CLIC(||)[e]
n-propylbenzene (**12**)	126	10.76	1.73	BL	LC	BL	d-CLIC	d-CLIC	d-CLIC
isopropylbenzene (**14**)	126	9.20	1.43	s-CLIC	s-CLIC(||)[e]	BL	d-CLIC	d-CLIC	s-CL
mesitylene (**6**)	127	8.65	1.00	TIC	s-CLIC	TIC	TIC	TIC	TIC
1,2,3-trimethylbenzene (**7**)	127	8.67	1.13	TIC	s-CLIC	TIC	TIC	TIC	TIC
1,2,4-trimethylbenzene (**8**)	127	8.87	1.20	s-CLIC	s-CLIC	s-CLIC	TIC	TIC,s-CLIC	s-CLIC
4-ethylnitrobenzene(**24**)	135	10.92	1.76	s-CLIC	s-CLIC	s-CLIC	s-CLIC	s-CLIC	s-CLIC
3,4-dimethylanisole (**22**)	139	9.78	1.41	BL	s-CLIC	s-CLIC(||)[e]	s-CLIC	s-CLIC(||)[e]	s-CLIC(||)[e]
3,5-dimethylanisole (**23**)	138	9.29	1.07	BL	s-CLIC	BL	s-CLIC	s-CLIC	s-CLIC
n-butylbenzene (**13**)	142	12.20	1.91	BL	d-CLIC	BL	d-CLIC	d-CLIC	d-CLIC
sec-butylbenzene (**15**)	142	9.12	1.30	BL	d-CLIC	d-CLIC	d-CLIC	d-CLIC	d-CLIC
tert-butylbenzene (**16**)	140	9.12	1.42	BL	s-CLIC(||)[e]	d-CLIC	d-CLIC	d-CLIC	d-CLIC
1,2,3,4-tetramethylbenzene (**9**)	143	8.89	1.19	TIC	s-CLIC	TIC	TIC	TIC	TIC
1,2,3,5-tetramethylbenzene (**10**)	143	8.89	1.11	TIC	s-CLIC	s-CLIC	TIC	s-CLIC	TIC
4-(dimethylamino)benzonitrile (**26**)	141	11.23	1.75	BL	LC	s-CLIC	s-CLIC	s-CLIC(||)[e]	s-CLIC(||)[e]
N,N-dimethyl-*3*-nitroaniline (**25**)	146	10.68	1.35	BL	LC	BL	s-CLIC(||)[e]	s-CLIC	s-CLIC

[a] V_{sulf} represents the molecular volume of the organomonosulfonates as calculated with Connolly surfaces in the Cerius[2] environment. V_{host} represents the sum of V_{sulf} and the volume of the guanidinium ion. [b] V_{guest} represents the molecular volume of the guest as calculated with Connolly surfaces in the Cerius[2] environment. [c] L_{guest} represents the length of the guest molecule as measured between the two most distal atoms, accounting for the van der Waals radius. [d] The guest eccentricity, e_{guest}, was calculated by dividing the maximum length by the molecular width, including van der Waals radii. The host/guest stoichiometries are 1:0.67 (CIC), 1:0.5 and 1:1 (sCLIC), and 1:0.5 (d-CLIC). s-CLIC(||) and s-CLIC(⊥) denote subclasses of the s-CLIC architecture in which the inclusion channels are parallel and perpendicular to the major ribbons, respectively.

produced a small number of GMS-based inclusion compounds with the s-CLIC and TIC frameworks (Figure 3).[30] The limited number of examples, however, precluded evaluation of the factors responsible for the formation of these architectures, prompting a search for new inclusion compounds based on the libraries in Scheme 1. Of the 624 possible host−guest combinations, 304 inclusion compounds were obtained in crystalline form. In cases for which inclusion was not observed, the expected guest-free compounds crystallized (i.e., identical to those described in the previous section), with no detectable amounts of other polymorphs by powder X-ray diffraction. Fully refined structures were determined for 42 of these compounds: 18 from our preliminary study and 24 new ones reported here (Table S2). The unit cells were determined for 15 additional compounds. X-ray powder diffraction analysis of compounds for which structures were fully refined or unit cells were obtained did not detect any polymorphs. Using these structure determinations as a basis, the architectures of most of the remaining compounds could be assigned through a combination of thermogravimetric analysis and ^{1}H NMR (determination of host/guest stoichiometry) and optical microscopy (identification of crystal habit, which was characteristic of the architecture). No polymorphs appear to be present for these compounds, although the possibility of small amounts cannot be entirely excluded. The inclusion compounds are described below according to the classification used for the guest-free compounds.

Group A: Para-Substituted Benzenesulfonates. GBS, **G4FBS**, **G4CBS**, **G4MBS**, **G4BBS**, and **G4IBS** formed 131 inclusion compounds out of 156 possible host/guest combinations in Scheme 1 (Table 2). Single-crystal XRD afforded satisfactory structural characterization for 41 of the 131 inclusion compounds. An additional 10 compounds were characterized by unit cell determinations. The GMS compounds with the larger halogen substituents, **G4CBS**, **G4BBS**, and **G4IBS**, formed inclusion compounds with nearly all 26 guests; only the **G4IBS**-isopropylbenzene combination failed to produce an inclusion compound. The halogenated host with the smallest L_{sulf} value, **G4FBS**, did not form inclusion compounds with some of the larger guest molecules, specifically *n*-propylbenzene (**12**), *N,N*-dimethyl-3-nitroaniline (**25**), and 4-(dimethylamino)benzonitrile (**26**). **GBS** and **G4MBS** did not include benzene, toluene,

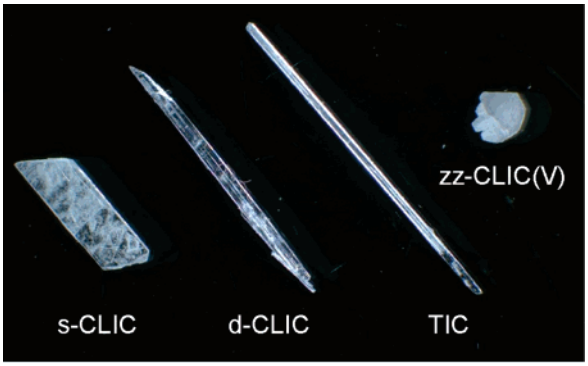

Figure 13. Photograph of single crystals of **G4BBS**·(*m*-xylene), **G4BBS**·0.5(*tert*-butylbenzene), **G4BBS**·0.67(*o*-xylene) and **G4TBBS**·0.67(benzene), which adopted the s-CLIC, d-CLIC, TIC, and zz-CLIC(V) architectures, respectively. Crystals of the zz-CLIC(IV) and zz-CLIC(V) have identical morphologies. Although crystals of d-CLICs and TICs grow as needles, the cross sections for the d-CLICs were rectangular, while the TICs were hexagonal. The long axes of the s-CLIC, d-CLIC, and TIC crystals were always parallel to the major GS ribbon axis. Following single-crystal structure determinations for a sufficient number of compounds with each architecture, most of the GMS inclusion compounds could be identified by crystal morphology, with corroboration by TGA (s-CLIC, monoclinic habit and either 1:1 or 1:0.5 host/guest stoichiometry; d-CLIC, needle habit with rectangular cross section and 1:0.5 host/guest stoichiometry; TIC, needle habit and 1:0.67 host/guest stoichiometry; zz-CLIC(IV), hexagonal-like plates and 1:0.67 host/guest stoichiometry: zz-CLIC(V), hexagonal-like plates and 1:0.5 host/guest stoichiometry).

ethylbenzene, *n*-propylbenzene, and *n*-butylbenzene molecules. Indeed, the **GBS** host, which has the smallest L_{sulf} value in this series, was highly discriminating, forming lamellar inclusion compounds only with guests having volumes within the range 110 Å^3 < V_{guest} < 135 Å^3.

The reduced occurrence of inclusion compounds for hosts with small L_{sulf} values is not entirely unexpected. The GS sheets of the GMS host framework can be viewed as "molecular jaws," in which organosulfonate groups projecting from opposing sheets close around the guest molecules. Guests that are large relative to L_{sulf} would tend to obstruct the approach of opposing sheets, thereby inhibiting intermolecular overlap between the organic components (host and guest) and reducing the cohesive energy required for crystallization. Under these conditions, formation of the guest-free compounds would become preferred. Interestingly, the aforementioned guest-free **G4BBS**, which exhibits the largest arene offset value of the guest-free bilayer compounds in group A, forms inclusion compounds with the largest range of guests. The large arene offset of **G4BBS** suggests this is the least stable of the guest-free bilayer compounds in this group, which would favor inclusion compound formation.

The majority of the inclusion compounds in group A adopted the s-CLIC architecture (84 of 131) for a surprisingly broad range of guest sizes and shapes. This architecture is constructed from the projection topology **PT-II**, identical to the guest-free s-CL architecture. Single-crystal structures and unit-cell determinations were used to verify the s-CLIC architecture for 31 of these compounds, which always grew as well-defined monoclinic plates. These were distinguished easily from the crystal habits exhibited by the other framework architectures (Figure 13), enabling confident assignment of the remaining 53 compounds on the basis of crystal morphology alone. The host/guest stoichiometries, which were either 1:0.5 or 1:1 for the s-CLICs, were consistent with these assignments.

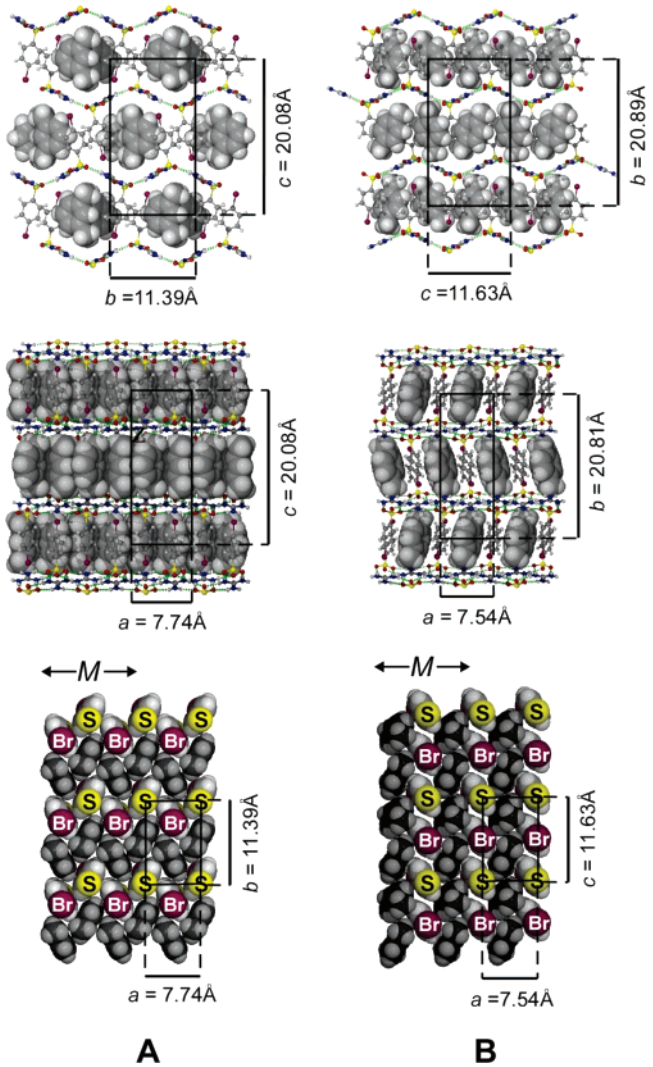

Figure 14. GMS inclusion compounds: (A) **G4BBS**·(toluene) and (B) **G4BBS**·(*m*-xylene) which adopted the s-CLIC architectures (**PT-II**) with inclusion channels aligned parallel and perpendicular to the major ribbon, respectively. Top and center panels depict side views parallel and transverse to the major ribbons, respectively. The bottom panels depict views perpendicular to the GS sheets, where the G ions and S oxygen atoms in the GS sheets have been removed to reveal the packing of the organic groups. In the upper and center panels, the host framework is depicted as wire-frame and the included guests as space-filled. In the lower panels the hosts and guests all are depicted as space-filled, but the guests are rendered with darker shading.

The s-CLIC framework assembled by interdigitation of organosulfonate groups from opposing GS sheets and guest molecules in the galleries. The **PT-II** topology creates channels on each sheet that are occupied by the organosulfonate groups from the opposing sheet, but yet are sufficiently large for inclusion of guest molecules as well (Figure 14). Of the s-CLICs characterized by single-crystal XRD, the channels are oriented either parallel or perpendicular to the major ribbon, the former occurring more often. In the parallel mode, interdigitated organomonosulfonate groups from opposing GS sheets exhibit edge-to-face contacts and form the walls of channels occupied by guests, which in turn adopt edge-to-face arrangements among themselves and with the organomonosulfonate groups. In the perpendicular mode, the channel walls consisted of interdigitated organomonosulfonate groups from opposing GS sheets arranged face-to-face, and guests organize face-to-face along the channel,

but the guests adopted edge-to-face arrangements with the organomonosulfonate groups.

A "double continuously layered inclusion compound" (d-CLIC) was observed in 18 of the 131 inclusion compounds in Group A. This architecture is constructed from projection topology **PT-III**, identical to the guest-free d-CL architecture. Single-crystal structures and unit cell determinations were used to verify the d-CLIC architecture for nine of these compounds, and the remaining nine compounds were assigned as d-CLICs by inspection of the crystal morphology, which was quite distinct (well-defined needles with rectangular cross sections; Figure 13). This architecture, which was limited to the bulkier guest molecules, displays a projection topology identical with the guest-free d-CL. Assuming a flat GS sheet, this configuration creates channels on each sheet surface that are twice as wide as the channels in the s-CLIC form, enabling interdigitation of organosulfonate groups from adjacent sheets with sufficient space remaining for the inclusion of even larger aromatic guests (Figure 15). Puckering of the sheets creates U-shaped pockets that are occupied by the bulky substituents (*n*-propyl, *n*-butyl, *i*-propyl, *tert*-butyl, *sec*-butyl) of the guests. Like the guest-free d-CL compounds, the d-CLIC puckering is defined by two puckering angles.

The topology of the d-CLIC architecture is the same as the GDS "double brick" architecture, which has been observed for only three GDS compounds.[21] The greater number of GMS d-CLIC compounds suggests that the absence of covalent connections between the GS sheets relaxes the constraints for puckering and structural registry between the sheets, thereby facilitating formation of the U-shaped cavities that accommodate bulky guest molecules. Because the host volumes of the s-CLIC and d-CLIC architectures are identical for a given organomonosulfonate, their total inclusion cavity volumes are identical as well. Consequently, the host/guest stoichiometry of the d-CLICs, which was favored by large guests, was always 1.0:0.5 rather than the 1:1 value observed for most of the s-CLICs.

Whereas GDS inclusion compounds are naturally restricted to lamellar architectures because of the covalent connections between adjacent sheets, the GMS hosts are not subject to this constraint. Certain host−guest combinations afforded morphologically distinct needles, with hexagonal cross-sections and often 2 cm long, during crystallization at the interface of a methanol solution containing the host components and neat guest (Figure 16). The habit of these crystals reflects the formation of TICs, in which the GS sheet curls into a cylinder consisting of six GS ribbons organized in the same quasihexagonal motif as the lamellar architecture (Figure 17). The organic groups attached to the sulfonate nodes project outward from the surface of each cylinder, generating the topology **CPT-II** (Figure 5). Interdigitation of these groups produces hexagonal arrays of cylinders, crystallizing in trigonal or hexagonal space groups ($P\bar{3}$ or $P6_3/m$). The cylinders can be viewed as puckered with $\theta_{IR} = 120°$, but with constant curvature instead of the accordion-like puckering of the lamellar architectures (negative curvature in the parlance of surfactant microstructures). The internal "pore" diameter, measured from the centers of atoms on opposite side of the cylinder, is slightly less than 12 Å, corresponding to an actual diameter of approximately 8.5−9 Å. Group A organomonosulfonates form TICs quite readily (41 of the 131 inclusion compounds).

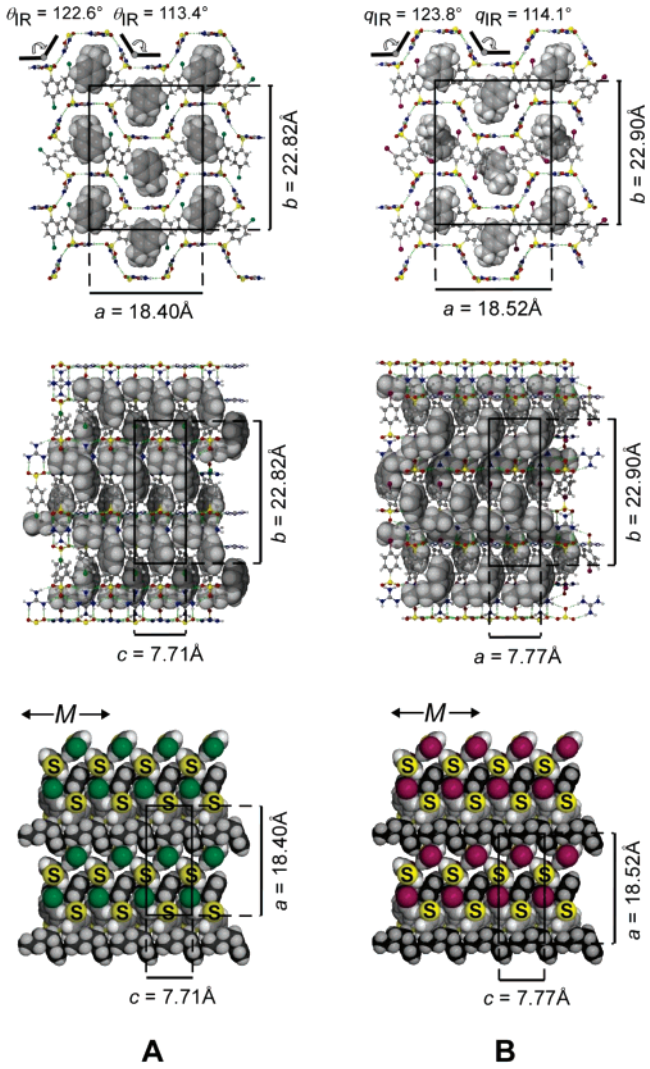

Figure 15. GMS inclusion compounds (A) **G4CBS**·0.5(butylbenzene) and (B) **G4BBS**·0.5(butylbenzene), which both adopt the d-CLIC architecture with projection topology **PT-III**. The top and center panels depict side views parallel and transverse to the major ribbons, respectively. The bottom panels depict views perpendicular to the GS sheets, where the G ions and S oxygen atoms in the GS sheets have been removed to reveal the packing of the organic groups. In the top and center panels, the host framework is depicted as ball-and-stick and the included guests as space-filled. In the lower panels the hosts and guests all are depicted as space-filled, but the guests are rendered with darker shading. The inter-ribbon puckering angles (θ_{IR}) are given in the top panels.

Each cylinder of the TICs contains uniformly spaced guest molecules stacked face-to-face along the length of the cylinder with an interplanar spacing of 3.72 Å. This value is equivalent to one-half the intraribbon sulfonate−sulfonate distance ($d_{S\cdots S}/2$) and signifies commensurate ordering of the guest molecules along the cylinder axis. The guests, however, exhibit 3-fold rotational disorder about the cylinder axis. Analysis of the residual electron density revealed that one-half of the guests are contained within the cylinders, as expected from the commensurate stacking (two guest molecules traverse the width of a band of six GS units along the cylinder axis). The remaining guest molecules are located in the interstices between the cylinders, resulting in the overall stoichiometry GMS·2/3(guest). The formation of the TIC architecture is somewhat surprising given that nonpolar guests are included inside cylinders with polar walls, suggesting commensurism and guest−guest interac-

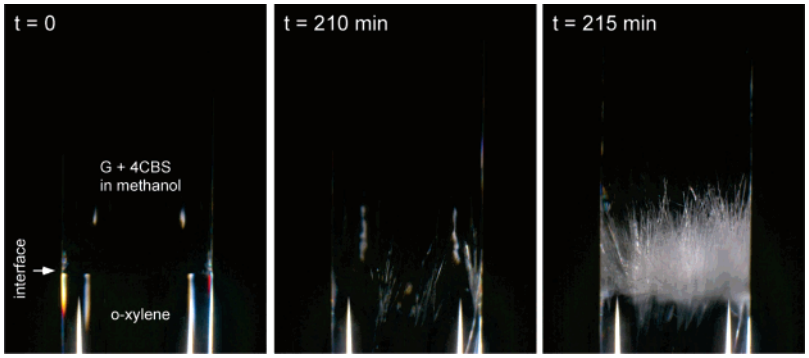

Figure 16. Snapshots of the crystallization of the TIC **G4CBS**·$^2/_3$(*o*-xylene) at the interface of a methanol solution, which contains the host components, and neat *o*-xylene. Rapid crystal growth was observed after a long induction time (the needle axis coincides with the long axes of the tubes).

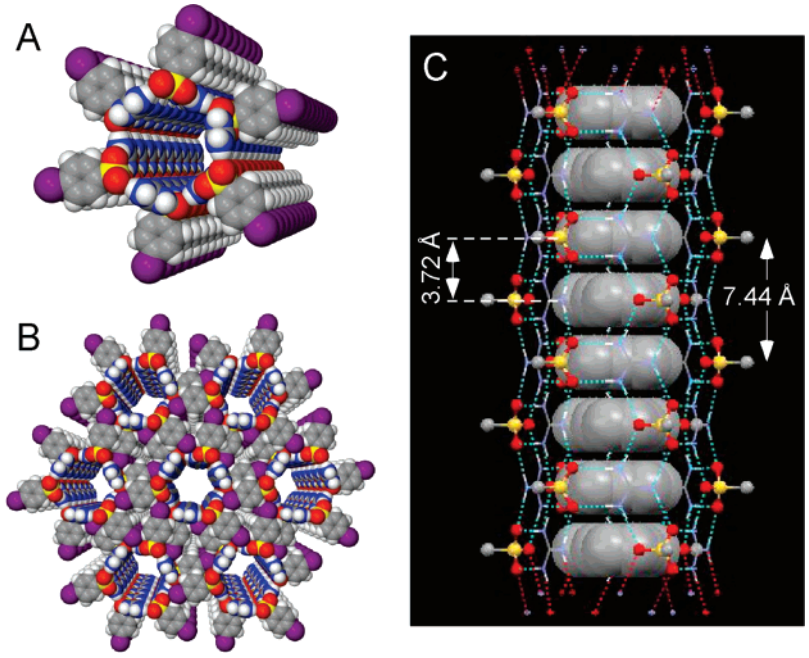

Figure 17. The tubular inclusion compound **G4BBS**·$^2/_3$(*o*-xylene): (A) model illustrating the quasihexagonal hydrogen bond connectivity of the GS network, which comprises six GS ribbons and forms the surface of the cylinder; (B) space filled rendering of a single cylinder, illustrating the outward projection of the **4BBS** groups and the roughly 8 Å tube diameter; (C) view perpendicular to the cylinder axis, illustrating the commensurism between the *o*-xylene guests (3.72 Å interplanar spacing) and the GS cylinder ($d_{S\cdots S}$ = 7.44 Å). The hydrogen atoms of the guests and all but the α-C atoms of the 4BBS molecules are omitted for clarity. The guanidinium ions are rendered as wireframe for better viewing of the guest molecules.

tions play an important role in the stability of these compounds. The inclusion of nonpolar guests in polar channels is not without precedent, however, as evidenced by the numerous examples of urea inclusion compounds formed with alkane guests.[44]

The most notable feature of the TICs is the tendency to incorporate disk-shaped guests, that is, guests with a low eccentricity (ϵ)[45] and volumes within the range 110 Å^3 < V_{guest} < 143 Å^3 (see below). The only exceptions were *N*,*N*-dimethylaniline and ethylbenzene, which have eccentricities of ϵ = 1.44 and 1.47, respectively. Interestingly, 11 of the 41 host−guest combinations that produced the TIC architecture afforded the s-CLIC architecture, albeit with different stoichiometries. This suggests that the TICs and CLICs have similar lattice energies.

Group B: Para-Substituted Benzenesulfonates with Bulky Substituents. G4EBS, **G4AS**, **G4NBS**, **G4IPBS**, **G4SBBS**, and **G4TBBS** formed 115 inclusion compounds out of 156 possible host/guest combinations based on the libraries in Scheme 1 (Table 3). Single-crystal structures were obtained for 14 of the 115 inclusion compounds, with an additional 7 characterized by unit cell determination. Single-crystal XRD and crystal morphology revealed that the **G4EBS**, **G4AS**, and **G4NBS** hosts adopted the s-CLIC architecture (**PT-II**) nearly exclusively. The lone exception was **G4EBS**·2/3(ethylbenzene), which adopted the TIC form (**CPT-II**).

Interestingly, the hosts with the bulkiest organosulfonates from this group—**G4IPBS**, **G4SBBS**, **G4TBBS**—included guests readily, producing 76 inclusion compounds out of a possible 78 combinations. Most of these inclusion compounds, however, did not form crystals suitable for single-crystal XRD or unit-cell determination (crystals were either too thin or diffracted poorly). Nonetheless, single-crystal XRD of a few compounds in this group, combined with morphology analysis and TGA,

(44) Hollingsworth, M. D.; Harris, K. D. M. In *Comprehensive Supramolecular Chemistry*; Atwood, J. L., Davies, J. E. D., MacNicol, D. D., Vögtle, F., Suslick, K. S., Eds.; Elsevier: Oxford, 1996; Vol. 6, pp 177−237.

(45) The eccentricity is a measure of the shape of a given guest molecule and is defined by the ratio of the maximum length to minimum width. Guest with an eccentricity of 1.0 are round disks such as benzene, while an eccentricity of 1.44 are ellipses such as ethylbenzene.

Table 3. Selected Structural Features of Guest Molecules and GMS Inclusion Compound Architectures for Organomonosulfonates in Groups B−D. (entries shaded in gray represent combinations that did not form inclusion compounds, such that only guest-free GMS compounds crystallized)

Guest	V_{guest} [b] (Å^3)	L_{guest} [c] (Å)	e_{guest} [d]	G4EBS	G4IPBS	G4sBBS	G4TBBS	G4AS	G4NBS	G2MBS	G3MBS	G2FBS	G3FBS	G2CBS	G3CBS	G2,4DMBS	G2,5DMBS	G3,4DMBS	G2,3,4TMBS	G2,4,5TMBS	G2,4,6TMBS
V_{sulf} [a] (Å^3)				148	165	181	181	145	143	134	137	126	127	134	133	151	149	150	168	167	173
V_{host} [a] (Å^3)				198	215	231	231	195	193	184	187	176	177	184	183	201	199	200	218	217	223
no guest	NA	NA	NA	s-CL(p)	BL	BL	d-CL	BL	s-CL(p)	s-CL	s-CL	BL	BL	BL	BL	s-CL	d-CL	s-CL	s-CL	s-CL	s-CL
1	82	6.97	1.01	s-CL(p)	BL	Lam	zz-CLIC(IV)	s-CLIC	s-CL(p)	s-CL	s-CL	BL	BL	BL	BL	s-CL	d-CL	s-CL	s-CL	s-CL	s-CL
2	97	7.98	1.25	s-CLIC	Lam	Lam	Lam	s-CLIC	s-CL(p)	s-CL	s-CLIC	BL	BL	BL	BL	s-CL	d-CL	s-CL	s-CL	s-CL	s-CL
21	105	9.22	1.43	s-CLIC	Lam	Lam	Lam	s-CLIC	s-CL(p)	s-CLIC	s-CL	BL	BL	BL	BL	s-CL	d-CL	s-CL	s-CL	s-CL	s-CL
11	110	9.50	1.44	TIC/s-CLIC	Lam	Lam	Lam	s-CLIC	s-CL(p)	s-CLIC	s-CL	BL	BL	BL	BL	s-CL	d-CL	s-CL	s-CL	s-CL	s-CL
18	110	7.70	1.09	s-CLIC	Lam	Lam	Lam	s-CLIC	s-CL(p)	s-CLIC	s-CLIC	BL	BL	BL	BL	s-CL	d-CL	s-CLIC	s-CL	s-CL	s-CL
17	112	7.72	1.08	s-CLIC	Lam	Lam	Lam	s-CLIC	s-CL(p)	s-CLIC	s-CLIC	BL	BL	BL	BL	s-CL	d-CL	s-CLIC	s-CL	s-CL	s-CL
3	113	7.44	1.06	s-CLIC	Lam	Lam	CLIC	s-CLIC	s-CL(p)	s-CLIC	s-CLIC	BL	BL	BL	BL	s-CLIC	d-CL	s-CLIC	s-CL	s-CL	s-CL
4	113	8.65	1.23	s-CLIC	Lam	Lam	Lam	BL	s-CLIC	s-CLIC	s-CLIC	BL	BL	BL	BL	s-CL	d-CL	s-CL	s-CL	s-CL	s-CL
5	111	8.89	1.38	s-CLIC	zz-CLIC(IV)	Lam	Lam	s-CLIC	s-CLIC	s-CLIC	s-CLIC	BL	BL	BL	s-CLIC	s-CLIC	d-CL	s-CL	s-CL	s-CL	s-CL
19	118	7.84	1.10	s-CLIC	Lam	Lam	CLIC	s-CLIC	s-CL(p)	s-CL	s-CL	BL	BL	BL	BL	s-CL	d-CL	s-CLIC	s-CL	s-CL	s-CL
20	124	9.21	1.44	s-CLIC	Lam	Lam	Lam	s-CLIC	s-CL(p)	s-CLIC	s-CLIC	BL	BL	BL	BL	s-CLIC	d-CL	s-CLIC	s-CL	s-CL	s-CL
12	126	10.76	1.50	s-CL(p)	Lam	Lam	zz-CLIC(IV)	BL	s-CL(p)	s-CL	s-CL	BL	BL	BL	BL	s-CL	d-CL	s-CL	s-CL	s-CL	s-CL
14	126	9.20	1.43	s-CL(p)	Lam	Lam	Lam	BL	s-CL(p)	s-CLIC	s-CLIC	BL	BL	BL	BL	s-CL	d-CL	s-CL	s-CL	s-CL	s-CL
6	127	8.65	1.00	s-CLIC	Lam	s-CLIC	Lam	BL	s-CL(p)	s-CLIC	TIC	BL	BL	BL	BL	s-CLIC	d-CL	s-CLIC	s-CL	s-CL	s-CL
7	127	8.67	1.06	s-CLIC	BL	Lam	Lam	BL	s-CLIC	s-CLIC	s-CLIC	BL	BL	BL	BL	s-CLIC	d-CL	s-CLIC	s-CL	s-CL	s-CL
8	127	8.87	1.14	s-CLIC	Lam	Lam	Lam	BL	s-CLIC	s-CLIC	s-CLIC	BL	BL	BL	s-CLIC	s-CL	d-CL	s-CLIC	s-CL	s-CL	s-CL
24	135	10.92	1.70	s-CLIC	Lam	Lam	Lam	s-CLIC	s-CL(p)	s-CLIC	s-CLIC	BL	BL	BL	BL	s-CL	d-CL	s-CL	s-CL	s-CL	s-CL
22	139	9.78	1.41	s-CLIC	zz-CLIC(IV)	Lam	Lam	s-CLIC	s-CL(p)	s-CL	s-CL	BL	BL	BL	BL	s-CLIC	d-CL	s-CLIC	s-CL	s-CL	s-CL
23	139	9.29	1.30	s-CL(p)	Lam	Lam	Lam	s-CLIC	s-CL(p)	s-CLIC	s-CLIC	BL	BL	BL	BL	s-CL	d-CL	s-CLIC	s-CL	s-CL	s-CL
13	142	12.20	1.56	s-CL(p)	Lam	Lam	zz-CLIC(IV)	BL	s-CL(p)	s-CLIC	s-CL	BL	BL	BL	BL	s-CL	d-CL	s-CL	s-CL	s-CL	s-CL
15	139	9.12	1.54	s-CL(p)	d-CLIC	Lam	Lam	BL	s-CL(p)	s-CLIC	s-CLIC	BL	BL	BL	BL	s-CL	d-CL	s-CL	s-CL	s-CL	s-CL
16	140	9.12	1.42	d-CLIC	Lam	Lam	Lam	BL	s-CL(p)	s-CLIC	s-CLIC	BL	BL	BL	s-CLIC	s-CL	d-CL	s-CL	s-CL	s-CL	s-CL
9	143	8.89	1.20	s-CLIC	Lam	Lam	Lam	BL	s-CLIC	s-CLIC	s-CLIC	BL	BL	BL	BL	s-CL	d-CL	s-CLIC	s-CL	s-CL	s-CL
10	143	8.89	1.02	s-CLIC	Lam	Lam	Lam	BL	s-CL(p)	s-CLIC	s-CLIC	BL	BL	BL	BL	s-CL	d-CL	s-CLIC	s-CL	s-CL	s-CL
26	141	11.23	1.75	s-CLIC	Lam	Lam	Lam	s-CLIC	s-CL(p)	s-CL	s-CL	BL	BL	BL	BL	s-CL	d-CL	s-CL	s-CL	s-CL	s-CL
25	146	10.68	1.35	s-CLIC	Lam	Lam	Lam	BL	s-CL(p)	s-CL	s-CL	BL	BL	BL	BL	s-CL	d-CL	s-CLIC	s-CL	s-CL	s-CL

[a] V_{sulf} represents the molecular volume of the organomonosulfonates as calculated with Connolly surfaces in the Cerius^2 environment. V_{host} represents the sum of V_{sulf} and the volume of the guanidinium ion. [b] V_{guest} represents the molecular volume of the guest as calculated with Connolly surfaces in the Cerius^2 environment. [c] L_{guest} represents the length of the guest molecule as measured between the two most distal atoms, accounting for the van der Waals radius. [d] The guest eccentricity, e_{guest}, was calculated by dividing the maximum length by the molecular width, including van der Waals radii. Lam refers to crystalline inclusion compounds that have lamellar architecture (s-CLIC, d-CLIC, zz-CLIC), but for which an unambiguous assignment was not possible. The host/guest stoichiometries are 1:0.67 (TIC), 1:0.5 and 1:1 (s-CLIC), 1:0.5 (d-CLIC), 1:0.67 (zz-CLIC(IV)), and 1:0.5 (zz-CLIC(V)). s-CL(p) denotes simple continuously layered in a polar space group.

permitted assignment of the framework architectures, which included s-CLIC (**PT-II**) and two new "zigzag" forms. **G4IPBS**·0.67(3,4-dimethylanisole) and **G4IPBS**·0.67(*p*-xylene), for which single-crystal structures were determined, adopted the zz-CLIC-(IV) architecture with the **PT-IV** topology. In contrast, the crystal structure of **G4TBBS**·0.25(1,4-di-*tert*-butylbenzene) revealed a **PT-V** topology with different projection sequences along the minor ribbons. The **PT-V** topology in this kind of inclusion compound, denoted zz-CLIC(V), contains inclusion cavities that can accommodate the shape of the 1,4-di-*tert*-butylbenzene guest molecules. The 3,4-dimethylanisole and *p*-xylene guest molecules in the zz-CLIC(IV) architecture are oriented perpendicular to the GS sheet (Figure 18). The length of the 1,4-di-*tert*-butylbenzene guest, however, precludes a perpendicular orientation, requiring larger and differently shaped cavities that allow the 1,4-di-*tert*-butylbenzene guest to lay with its long axis parallel to the GS sheet. The large footprint of the 1,4-di-*tert*-butylbenzene guest is reflected in its 1:0.5 host/guest stoichiometry. Only one host−guest combination from this group, **G4IPBS**·0.5(*sec*-butylbenzene), could be confirmed as the d-CLIC architecture by single-crystal XRD. The projection sequence along the major ribbons and the puckering of the GS

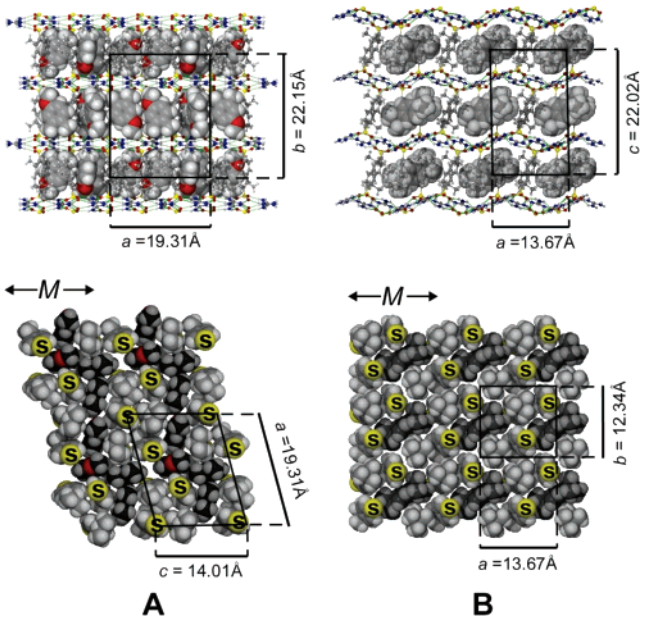

Figure 18. GMS inclusion compounds: (A) **G4IPBS·**(3,4-dimethylanisole), which adopts the zz-CLIC(IV) architecture with the **PT-IV** projection topology. (B) **G4TBBS·**(1,4-di-*tert*-butylbenzene), which adopts the zz-CLIC(V) architecture with the **PT-V** topology. The top panels represent side views parallel to the major ribbons. The bottom panels depict views perpendicular to the GS sheets, where the **G** ions and **S** oxygen atoms in the upper GS sheet have been removed to reveal the packing of the organic groups. In the upper panels, the host framework is depicted as ball-and-stick and the included guests as space-filled. In the lower panels the hosts and guests all are depicted as space-filled, but the guests are rendered with darker shading.

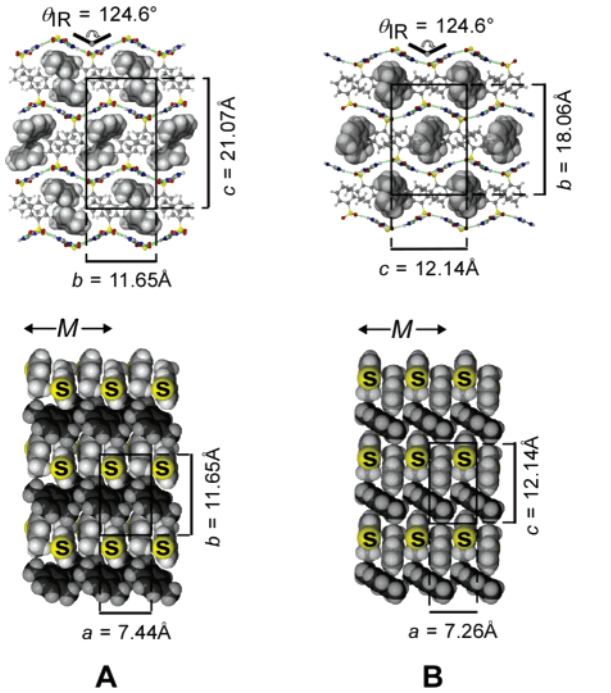

Figure 19. GMS inclusion compounds (A) **G3MBS·**(*p*-xylene) and (B) **G2MBS·**0.5(1,2,3,4-tetramethylbenzene), which both adopt the s-CLIC architecture with the **PT-II** projection topology. The bottom panels depict views perpendicular to the GS sheets, where the **G** ions and **S** oxygen atoms in the upper GS sheet have been removed to reveal the packing of the organic groups. In the upper panels, the host frameworks are depicted as ball-and-stick and the included guests as space-filled. In the lower panels the hosts and guests all are depicted as space-filled, but the guests are rendered with darker shading. θ_{IR} represents the interribbon puckering angle. The guest disorder in panel B has been removed for clarity.

sheet combine to create U-shaped pockets occupied by the bulky *sec*-butyl substituents of the guests.

Unlike all other host−guest combinations, the correlation of crystal morphology with crystal architecture for **G4IPBS**, **G4SBBS**, **G4TBBS** inclusion compounds, as determined by single-crystal XRD, was found to be unreliable. For these three hosts, the s-CLICs, zz-CLICs, and d-CLICs that could be characterized by X-ray diffraction crystallized as very thin plates or clusters of microcrystals. Many crystals were small and poorly shaped, to the extent that a credible characterization of crystal morphology was not feasible. This precluded assignment of the framework architecture for many of the host−guest combinations in this subgroup. These unassigned compounds, which account for 67 of the 78 possible host/guest combinations from these three hosts, are designated only as "Lam" (i.e., lamellar) in Table 3.

Group C: Ortho- and Meta-Substituted Benzenesulfonates. **G2MBS**, **GMFBS**, **G2CBS**, **G3CBS**, **G2FBS**, and **G3FBS** formed 39 inclusion compounds out of 156 possible host/guest combinations based on the libraries in Scheme 1 (Table 3). Although single-crystal XRD was performed on only two of the 39 inclusion compounds, **G2MBS·**(1,2,3,4-tetramethylbenzene) and **G3MBS·**(*p*-xylene), it was apparent from the well-defined crystal habits that these and the remaining compounds adopted the s-CLIC architecture (**PT-II**). The formation of inclusion compounds with GMS hosts having meta and ortho substituents on the arenesulfonate rings was sensitive to the nature of the substituents. The halogenated compounds **G2FBS**, **G3FBS**, **G2CBS** did not form inclusion compounds, preferring instead to form their guest-free bilayer phases. **G3CBS** formed inclusion compounds with only three guests (*p*-xylene, 1,2,4-trimethylbenzene, *tert*-butylbenzene), each crystallizing in the s-CLIC architecture. **G2MBS** and **G3MBS**, however, form 36 inclusion compounds out of a possible 52 combinations. The single-crystal structures of **G2MBS·**(1,2,3,4-tetramethylbenzene) and **G3MBS·**(p-xylene) revealed the s-CLIC architecture (Figure 19). Unlike the s-CLIC inclusion compounds in group A (para substituted organosulfonates), the presence of ortho and meta substituents obstruct edge-to-face packing of the interdigitated organosulfonate groups from opposing sheets. Instead, the host arene rings stack face-to-face to form the walls of channels oriented parallel with the major ribbon of the s-CLIC topology. The guest molecules organized as inclined stacks in these channels, exhibiting edge-to-face packing with the arene rings of the host.

Group D: Multiply Methyl Substituted Benzenesulfonates. Of the six GMS compounds in this group—**G2,4DMBS**, **G2,5DMBS**, **G3,4DMBS**, **G2,3,4TMBS**, **G2,4,5TMBS**, and **G2,4,6TMBS**—only **G2,4DMBS** and **G3,4DMBS** formed inclusion compounds, and only with a rather small number of guest molecules from Scheme 1 (19 inclusion compounds of a possible 156; see Table 3). The reduced ability of this group to include guests most likely reflects the large volume of the organosulfonate groups, which could inhibit inclusion by the host frameworks. Except for *p*-xylene and 3,4-dimethylanisole, the guests included by **G2,4DMBS** and **G3,4DMBS** were found to template TIC architectures for the para-substituted benzenesulfonates in group A. This indicates that the presence of a second methyl group on the arenesulfonate is sufficient to

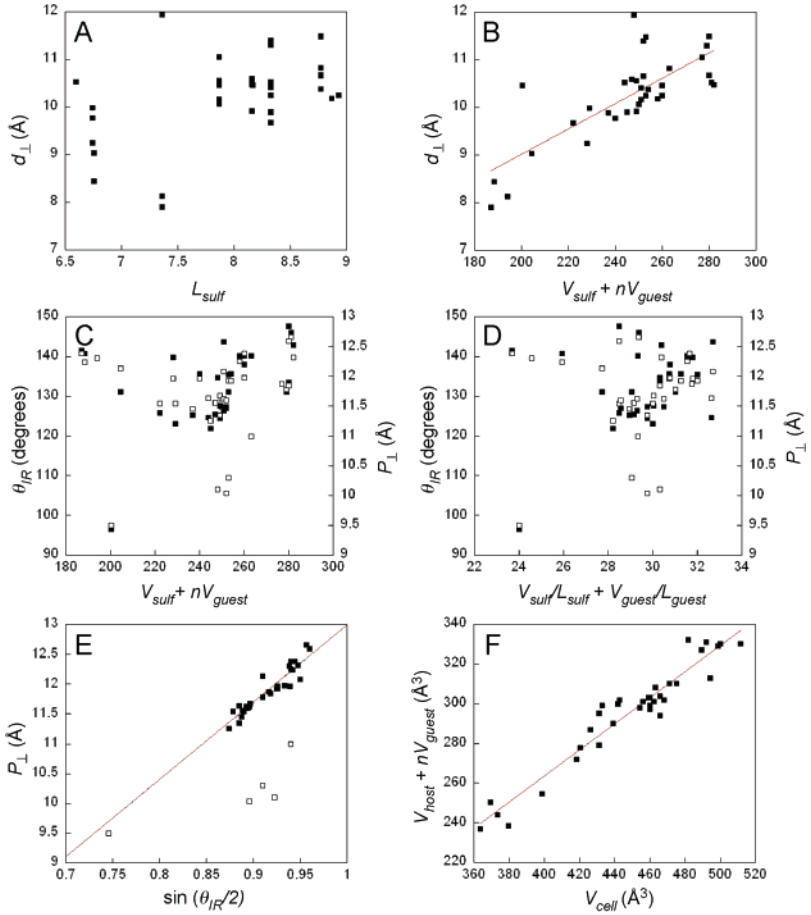

Figure 20. Metric relationships between select structural parameters for GMS inclusion compounds with the s-CLIC architecture. (A) Unlike the guest-free compounds, no discernible trend is observed for the dependence of $d_\perp$ on L_{sulf}. (B) Dependence of $d_\perp$ on the combined volume of the organosulfonate and the guest molecules, tantamount to a swelling of the lamella. The line represents a least-squares fit to all the data. (C) θ_{IR} (□) and $P_\perp$(■) exhibit no obvious correlation with the combined volume of the organosulfonate and the guest molecules. (D) Likewise, θ_{IR} (□) and $P_\perp$(■) are not correlated with the combined "footprint areas" calculated from $V_{sulf}/L_{sulf} + nV_{guest}/L_{guest}$. (E) $P_\perp$ exhibits a linear dependence on sin(θ_{IR}/2) for most of the GMS s-CLICs, as expected from eq 1b. The solid line represents a least-squares fit of these variables for the compounds corresponding to the filled squares only. The slope and intercept of this fit are 13.3 and 0.3 Å, nearly identical to the values expected from eq 1b.[46] (F) A plot of $V_{host} + nV_{guest}$ and V_{cell} produces a slope of $m = 0.66$, which represents the average packing fraction for the s-CLICs.

frustrate the formation of the TIC architecture, reflecting rather stringent requirements for interdigitation-driven assembly of the cylinders.

Structural Trends. The frequency of inclusion compound formation decreases in the order group A (131/156) > group B (115/156) > group C (39/156) > group D (19/156), a trend that reflects more facile guest inclusion for para-substituted benzenesulfonates and a reduced tendency for inclusion with increasing V_{sulf} and awkwardly shaped organomonosulfonates. The introduction of ortho and meta substituents clearly frustrates guest inclusion, as gleaned from the entries on the right side of Table 3 (guest-free only combinations are shaded gray). The role of shape was apparent from the large number of inclusion compounds formed by the para-substituted **G4IPBS**, **G4AS**, and **G4TBBS**; even though these hosts have large V_{sulf} values, they readily form lamellar inclusion compounds.

The large number of inclusion compounds that crystallize with the s-CLIC architecture permits examination of certain metric relationships in a manner similar to that for the guest-free s-CL compounds. Unlike the guest-free compounds, however, many of these metric relationships are not well behaved. For example, the dependence of $d_\perp$ on L_{sulf}, does not display any discernible trend (Figure 20A). This is understandable as the guest molecules also exert an influence on the lamellar spacing, masking the contribution of L_{sulf}. On the other hand, the values of $d_\perp$ do exhibit a reasonable correlation with the combined volume of the host and guests (Figure 20B), signifying an effective "swelling" of the galleries as the combined volume of the organic moieties, $V_{sulf} + nV_{guest}$, is increased. No apparent correlations between θ_{IR} or $P_\perp$ and either $V_{sulf} + nV_{guest}$ or $V_{sulf}/L_{sulf} + V_{guest}/L_{guest}$ (the area of the "footprint") can be gleaned (Figure 20C, 20D). The most plausible explanation for the poor correlations between these variables is the absence of any constraints on orientations of the guest molecules, which are not appended to the GS sheet. This extra degree of freedom permits a variety of packing motifs among the organomonosulfonates and the guests, to the extent that the puckering angles cannot be expected to depend on volume alone. Similarly, the footprint areas deduced from V_{guest}/L_{guest} presumes that the long axes of the guest molecules are perpendicular to the GS sheet, which is not observed in all s-CLIC compounds.

Except for a few outliers, the dependence of $P_\perp$ on sin(θ_{IR}/2), is linear and conforms to eq 1b (Figure 20E). Like the guest-free s-CL compounds, this indicates that the puckering-induced contraction of the lattice along $P_\perp$ in response to the packing of the organic components occurs without any substantial

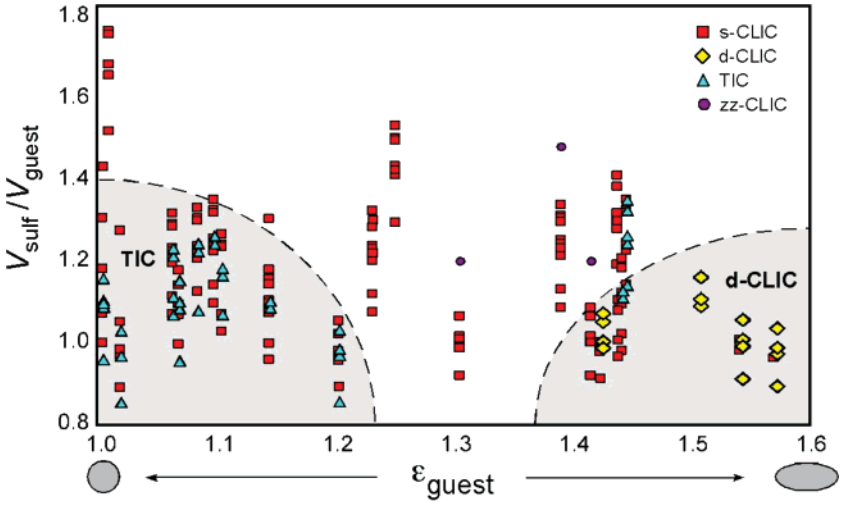

Figure 21. Structural phase diagram for GMS inclusion compounds using V_{sulf}/V_{guest} and ϵ_{guest} as independent variables. This plot contains 206 data points representing unique host−guest combinations. Some of the data points are obscured by overlap. Because the **G4IPBS**, **G4sBBS**, and **G4TBBS** inclusion compounds could not be assigned to specific lamellar architectures, these are not included in the figure.

contributions from other structural distortions. Unlike the guest-free compounds, the values of $P_\perp$ are nearly identical to those expected for ideal puckering with a value of 6.5 Å assigned to the ribbon width. The linearity in Figure 20E does not contradict the conclusions reached from the data in panels C and D, as $P_\perp$ and $\sin(\theta_{IR}/2)$ are linked through the geometric changes in the lattice as it responds to the packing orientations and volume of the various organic components. Comparison of Figures 20E and 12A reveals that the θ_{IR} values are larger overall in the inclusion compounds (i.e., less puckering) compared with the guest-free compounds, with some inclusion compounds having θ_{IR} values approaching 180°. This behavior simply reflects the expansion of the framework to accommodate the extra volume introduced by the guests. Figure 20F illustrates uniform packing fractions for a large number of s-CLIC compounds, reflecting a tendency toward constant packing densities made possible by puckering of the compliant GS framework and packing freedom introduced by unrestrained guests.

Architectural Sorting and Soft Matter Correspondence. Guest-free compounds were observed for every organomonosulfonate in Scheme 1. Formation of a GMS inclusion compound always competes with formation of its corresponding guest-free phase and, unlike the pillared GDS frameworks, inclusion cavity formation is not predestined. The formation of 304 out of 624 possible host−guest combinations therefore seems quite remarkable. The propensity to form inclusion compounds certainly can be attributed to the unique ability of the GS sheets to pucker, effectively enabling a host framework to "shrink-wrap" about guest molecules so that reasonable packing densities of the organic host groups and the guests can be achieved. Furthermore, the GMS hosts can adopt a variety of lamellar architectures with differently sized and shaped inclusion cavities that can accommodate a wide range of guests, and rotation about the C−S bond in the organosulfonate groups permits further optimization of the host−host and host−guest packing. These modes of structural adaptability, however, also are available to the guest-free phases. The principal differences between the guest-free and inclusion compounds are (i) the presence of unconstrained guest molecules that are not anchored to the GS sheet, which can increase the degree of freedom for intermolecular packing among the organic constituents, thereby creating conditions favorable for packing arrangements between the GS sheets that are superior to those in the guest-free phases, and (ii) the absence of a covalent connection between the GS sheets, which removes the constraint of registry between adjacent sheets, thereby allowing opposing GS sheets to "float" parallel and perpendicular to the layers so that packing with guest molecules can be optimized. Perhaps, therefore, it is not surprising that the proclivity of the GMS compounds for inclusion rivals that of the GDS hosts. The TIC architecture, which is not possible for the GDS frameworks, provides an additional avenue to the formation of GMS inclusion compounds.

The extraordinary number of GMS inclusion compounds derived from a common hydrogen-bonded network creates a unique, possibly unparalleled, opportunity for systematic examination of the relationship between the structures of the molecular components and crystal structure. Using the 206 GMS inclusion compounds for which framework architectures could be assigned, a structural "phase diagram" can be constructed to sort the various architectural isomers according to well-defined, simple molecular parameters, specifically the sulfonate volume/guest volume ratio, V_{sulf}/V_{guest}, and the guest eccentricity, ϵ_{guest}, both measured readily from molecular models (Figure 21). The guest eccentricity, defined as the length of the guest divided by its width after accounting for van der Waals radii, ranges from $\epsilon_{guest} = 1.0$ (benzene) to $\epsilon_{guest} = 1.75$ (4-ethylnitrobenzene). The TIC and d-CLIC architectures reside primarily in separate sectors. The TIC architecture was preferred for guests that are smaller and disk-shaped, as these fit more comfortably in the highly symmetric cylinders and are more suitable templates for the cylindrical geometry. The host−guest combinations producing the TIC architecture occupy a phase region bounded by $0.8 < V_{sulf}/V_{guest} < 1.3$ and values between $1.0 < \epsilon_{guest} < 1.2$. Only *N*,*N*-dimethylaniline (**20**, $\epsilon_{guest} = 1.44$), which forms TICs with **G4CBS** and **G4BBS**, and ethylbenzene (**11**, $\epsilon_{guest} = 1.47$), which forms TICs with **G4FBS**, **G4CBS**, **G4BBS**, and **G4IBS**, lie outside the TIC sector.[47]

(46) The open squares are regarded as outliers (**G4FBS·(20)**; **G4BBS·(4)**; **G4IBS·(4)**; **G4IBS·(20)**). If the open squares are included in the least squares fit, the slope and intercept do not change appreciably (13.2 and 0.4 Å, respectively) but the regression coefficient is reduced from $R = 0.94$ to $R = 0.69$.

Except for **G4EBS**·2/3(ethylbenzene), the TIC architecture was not observed for organosulfonates in groups B−D. Bulky substituents on the organomonosulfonate ring (large V_{sulf}) appear to frustrate the interdigitation required for intercylinder packing; this defines the upper boundary of the TIC sector. The s-CLIC architecture, however, appears across much of the phase diagram. This can be attributed to the facile puckering of the s-CLIC framework, which makes this framework sufficiently pliable to accommodate a broad range of guest molecules. The s-CLICs are absent, however, for $\epsilon_{guest} > 1.45$, at which the d-CLICs are overwhelmingly favored. The host−guest combinations producing the d-CLIC architecture are located at the lower right of the diagram, in a sector bounded by $1.4 < \epsilon_{guest} < 1.6$ and $0.8 < V_{sulf}/V_{guest} < 1.2$. The five guests that promote this architecture—*n*-propylbenzene (**12**), *n*-butylbenzene (**13**), isopropylbenzene (**14**), *sec*-butylbenzene (**15**), and *tert*-butylbenzene (**16**)—apparently are unable to fit within the relatively narrow inclusion channels of the s-CLIC framework or the relatively small cylinders of the TICs. These examples illustrate that the d-CLIC framework, with its wider U-shaped channels, is better able to accommodate larger guest molecules with an elliptical shape. Overall, Figure 21 reveals that the large number of host−guest combinations explored here permits grouping of the inclusion compound architectures according to the shape of the guests and the relative volumes of the organomonosulfonate groups, enabling more reliable structure prediction for this class of compounds than for molecular crystals in general.

The isomerism displayed by the various CLICs and TICs is somewhat reminiscent of "soft matter,"[31] specifically lamellar and hexagonal cylinder phases observed in aqueous surfactant assemblies and block copolymers.[32,34,35] Distinct polar (i.e., the GS sheet) and nonpolar (the organosulfonate groups and guest molecules) regions define the GMS guest-free and inclusion compounds, similar to the segregation observed in soft matter microstructures. This correspondence is even more apparent for guanidinium phenylalkanesulfonates, biphenylalkanesulfonate, and alkanesulfonates, which are crystalline with lamellar architectures at room temperature and form smectic liquid crystal phases upon heating and lamellar organogels in certain organic solvents.[48−51] Like soft matter microstructures, the GMS inclusion compounds are equipped with a well-defined, elastic interface, the GS sheet, that is common to both the lamellar and hexagonal architectures. In the case of the TICs, the GS sheet curls into a closed cylinder, generating a structure that resembles the H_{II} inverse hexagonal phases for surfactant microstructures. Whereas the "lamellar" CLICs can be viewed as having zero mean curvature and zero Gaussian curvature, the TICs can be viewed as having negative mean curvature and zero Gaussian curvature.[52] As noted by Seddon,[32] an inextensible yet flexible surface (e.g., a sheet of paper) can be deformed easily into a shape of arbitrary mean curvature, but only if the Gaussian curvature remains zero. The GS sheet represents a supramolecular hydrogen-bonded version of this kind of surface, deforming into a cylinder while the curvature along the cylinder axis remains zero. The curvature spreads the organic groups on the outer surface of the cylinder to allow interdigitation of neighboring cylinders. Finally, the structural phase diagram in Figure 21 is not unlike soft matter microstructure phase diagrams, which also are based on relatively simple parameters.[53] The length-scale defining curvature and periodicity in soft matter is larger, however, typically ranging from tens to hundreds of nanometers.

Although high-symmetry space groups that demand curvature (i.e., cubic, hexagonal) are common in soft matter, most small molecules crystallize in low-symmetry space groups (i.e., triclinic, monoclinic). The space group constraints on molecular crystals can be gleaned from a search of the Cambridge Structural Database (v5.28, November 2006 release), which indicated that of 390081 entries, only 4437 (1.1%) were trigonal/hexagonal and 1895 (0.5%) were cubic. These statistics reflect the incompatibility between the low point-group symmetry characteristic of molecules and the special positions in high-symmetry space groups. This constraint is circumvented in soft matter because the interface that defines the separation between the dissimilar components is very elastic and the radii of curvature are large, to the extent that the supramolecular aggregates can conform about the high-symmetry special positions with minimal energetic penalty at the local level. The symmetry constraints are relaxed further in soft matter because disordered molecular aggregates sit on special positions. Of the 304 inclusion compounds generated from the libraries in Scheme 1, 42 (14%) crystallized as TICs with trigonal or hexagonal space-group symmetry. This high frequency of occurrence can be attributed to soft matter-like elastic character of the GS sheet, an aggregate of molecules that deforms into cylinders situated about key special positions[54] in the trigonal or hexagonal systems. Furthermore, although the GS sheet is crystallographically ordered, the organosulfonate groups, intracylinder guests, and intercylinder guests are disordered, which relaxes the symmetry constraints imposed by $\bar{3}$, $\bar{6}$, *m*, and *i* special positions.

We note that hexagonal crystal symmetry has been observed in $(H_3O)[V_3O_4](H_2O)(PhPO_3)_3]\cdot 2.33H_2O$, which crystallizes in the hexagonal $P\bar{3}$ space group as cylinders assembled into hexagonal arrays through interdigitation of phenyl rings that project from their outer surfaces, not unlike the TIC architecture. This compound, however, appears to be an isolated example in a class of compounds that typically exhibit lamellar structures.[55] The well-documented urea inclusion compounds (UICs) crystal-

(47) The idealized length of *N*,*N*-dimethylaniline and ethylbenzene (9.21 and 9.50 Å, respectively), is somewhat longer than the internal diameter of the cylinder based on the van der Waals diameter. The single crystal structures of these compounds, although poorly refined, support the presence of face-to-face stacks of guest molecules within the cylinder, but the poor refinement for these structures has prohibited an accurate determination of the orientation of the aromatic rings or the disposition of the substituents.

(48) Mathevet, F.; Masson, P.; Nicoud, J.-F.; Skoulios, A. *Chem. Eur. J.* **2002**, *8*, 2248.

(49) Martin, S. M.; Yonezawa, Y.; Horner, M. J.; Macosko, C. W.; Ward, M. D. *Chem. Mater.* **2004**, *16*, 3045.

(50) Martin, S. M.; Ward, M. D. *Langmuir*, **2005**, *21*, 5324.

(51) Mathevet, F.; Masson, P.; Nicoud, J.-F.; Skoulios, A. *J. Am. Chem. Soc.* **2005**, *127*, 9053.

(52) The mean and Gaussian curvatures are defined as $H = 1/2(c_1 + c_2)$ and $K = c_1c_2$, respectively, where c_1 and c_2 are the principal curvatures at a point on the surface ($c_1 = c_2 = 0$ for CLICs; c_1 = negative, $c_2 = 0$ for TICs).

(53) Surfactant−water microstructures are governed by the volume (*V*) of the hydrophobic chain of the surfactant, the area (*a*) of the hydrophilic head group, and the length (*l*) of the hydrocarbon chain. Block copolymer microstructures are governed by the immiscibility of the dissimilar segments, described by the Flory−Huggins parameter χ, the molecular weight *N*, and the relative volume fractions of the dissimilar segments, which are presumed to behave as random coils.

(54) The center of the cylinders coincide with key special positions in the trigonal or hexagonal space groups $P\bar{3}$, No. 147: 3-fold axis at $^1/_3$, $^2/_3$, $^1/_4$; $^2/_3$, $^1/_3$, $^3/_4$; $^2/_3$, $^1/_3$, $^1/_4$; $^1/_3$, $^2/_3$, $^3/_4$ and $^1/_3$, $^2/_3$, $\bar{z}$; $P6_3/m$, No. 176: $\bar{6}$ at $^1/_3$, $^2/_3$, $^1/_4$; $^2/_3$, $^1/_3$, $^3/_4$; $^2/_3$, $^1/_3$, $^1/_4$; $^1/_3$, $^2/_3$, $^3/_4$.

(55) Bonavia, G.; Haushalter, R. C.; O'Connor, C. J.; Sangregorio, C.; Zubieta, J. *Chem. Commun.* **1998**, 2187.

lize in hexagonal or near-hexagonal symmetry through the formation of hydrogen-bonded cylinders,[56] but these do not display the lamellae-cylinder isomerism exhibited by the GMS compounds. Perhydrotriphenylene and tris(o-phenylenedioxy)-spirocyclotriphosphazene form cylindrical host lattices with hexagonal space group symmetry through van der Waals interactions,,[57−60] as do guest-free phases of various alkoxy-substituted triphenylenes.[61] In these examples, however, the high space-group symmetry results from propagation of the threefold point-group symmetry of the molecular constituents, whereas the trigonal/hexagonal order in the TICs stems from curvature of the 2D GS network into cylinders of hexagonal symmetry.

The structural resemblance of GMS inclusion compounds to soft matter lamellar and hexagonal phases prompts the question of whether concepts of amphiphile segregation, volume fraction of dissimilar components, curvature, and interfacial tension can be used, in general, to describe the solid-state structure of molecular crystals. A structural correspondence between crystal structures and soft matter microstructures has been invoked for Ag^+-based coordination networks, generated from various polynitrile ligands, which formed cylindrical, perforated layer, lamellar, gyroid network topologies.[62,63] Periodic minimal surfaces, on which the curvature vanishes on every point on the surface,[64] have been invoked for inorganic networks comprising atoms of different sizes, which pack more efficiently on a curved surface than on a plane.[65] The structure of some inorganic compounds has been described in terms of periodic equipotential or zero-potential surfaces.[66] Periodic minimal surfaces also were invoked for a metal−organic framework that crystallized in a cubic space group.[67] Constant curvature and minimal surface concepts invoked in these cases can provide a convenient way to visualize space partitioning and structural order,[68] but inorganic and metal−organic networks typically do not possess deformable elastic interfaces that are the signature of soft matter microstructures, and the network topologies reflect the propagation of the local symmetries. Perhaps more interesting in this regard are molecular crystals that assemble through "soft" and less directional intermolecular forces, such as van der Waals and hydrogen bonding.[69] Constant curvature surfaces and polar/nonpolar volume ratios have been used to describe the structures of various aromatic polyethers, polyalcohols, aromatic and cyclohexylammonium carboxylates, and ether−thioethers.[63] Hydrogen-bond networks and a large unit cell appear to play a role in the formation of one of only two single-component compounds with the cubic $Ia\bar{3}d$ space group (No. 230).[70] A hydrate of a calix[4]resorcinarene has been reported to crystallize (with nitrobenzene solvent molecules) in the cubic $I432$ space group,[71] each unit cell containing an octahedral cubic spheroid assembled through 60 O···H···O hydrogen bonds that produce a structure with "saddle surfaces" of zero mean curvature and zero Gaussian curvature. Compounds like these seem to support the notion that high space-group symmetries are more likely for molecular aggregates assembled by soft intermolecular interactions, such as hydrogen bonds. Interestingly, lattices constructed from the centers of the atomic positions of small molecules in low-symmetry space groups closely resemble hexagonal or cubic close-packed lattices, suggesting that the packing in many molecular crystals approaches high space-group symmetry.[72] This is underscored by a recent analysis of the CSD and the Protein Data Bank (PDB) that determined that a plurality of proteins crystallizing in hexagonal space groups exhibit a c/a ratio of $(8/3)^{1/2}$, characteristic of sphere-packing.[73]

Conclusion

The observation of 304 inclusion compounds out of a possible 624 host−guest demonstrates the remarkable versatility of the GMS compounds as host materials. Unlike the related guanidinium organodisulfonate compounds, inclusion by GMS compounds is not "predestined" as cavities between adjacent sheets are not enforced by covalent connections provided by the disulfonate pillars. Instead, the formation of inclusion compounds in GMS hosts relies on collective, noncovalent dispersive interactions among the arene rings of the hosts and guests, including host−host, guest−guest, and host−guest interactions. The GS sheets of the lamellar GMS host frameworks can be viewed as "molecular jaws," in which the organosulfonate groups projecting from opposing sheets close around the guest molecules. The ubiquity of the lamellar GMS inclusion compounds and their crystal structures suggests that introduction of guest molecules, which are not anchored to the GS sheet, reduces packing constraints and facilitates the achievement of more optimum packing modes, thereby providing an enthalpic benefit compared with the guest-free phases. The persistence of the GS network allows a comprehensive examination of the effect of interchanging hosts and guests in a systematic manner. The distinction between the GMS and GDS inclusion compounds is most apparent from the formation of the hexagonal TIC architecture, in which the use of a organo*mono*sulfonate allows constant curvature into cylinders, which is not possible for GDS frameworks. To our knowledge, the observation of lamellar and cylindrical architectures that are related through curvature by a common elastic 2D network (i.e., the GS sheet) is unique among molecular crystals. Furthermore, the classification of crystal architectures according to simple molecular variables, though common for soft matter, is rare for molecular

(56) (a) Harris, K. D. M. *J. Solid State Chem.* **1993**, *106*, 83. (b) Harris, K. D. M. *Chem. Soc. Rev.* **1997**, *26*, 279.
(57) Allegra, G.; Farina, M.; Immirzi, A.; Colombo, A.; Rossi, U.; Broggi, R.; Natta, G. *J. Chem. Soc. B* **1967**, 1020.
(58) (a) Allcock, H. R.; Levin, M. L.; Whittle, R. R. *Inorg. Chem.* **1986**, *25*, 41. (*b*) Allcock, H. R.; Primrose, A. P.; Sunderland, N. J.; Rheingold, A. L.; Guzei, I. A.; Parvez, M. *Chem. Mater.* **1999**, *11*, 1243.
(59) Primrose, A. P.; Parvez, M.; Allcock, H. R. *Macromolecules* **1997**, *30*, 670.
(60) Comotti, A.; Simonetti, R.; Catel, G.; Sozzani, P. *Chem. Mater.* **1999**, *11*, 1476.
(61) Andersen, T. L.; Krebs, F. C.; Thorup, N.; Bechgaard, K. *Chem. Mater.* **2000**, *12*, 2428.
(62) Mallik, A. B.; Lee, S.; Lobkovsky, E. B. *Cryst. Growth. Des.* **2005**, *5*, 609.
(63) Xu, Z.; Kiang, Y.-H.; Lee, S.; Lobkovsky, E. B.; Emmott, N. *J. Am. Chem. Soc.* **2000**, *122*, 8376.
(64) Anderson, D. M; Davis, H. T.; Scriven, L. E.; Nitsche, J. C. C. *Adv. Chem. Phys.* **1990**, *77*, 337.
(65) (a) Andersson, S. *Angew. Chem., Int. Ed. Engl.* **1983**, *22*, 69. (b) Andersson, S.; Hyde, S. T.; Larsson, K.; Lidin, S. *Chem. Rev.* **1988**, *88*, 221.
(66) (a) Nesper, R.; von Schnering, H. G. *Z. Kristallogr.* **1985**, *170*, 138. (b) Nesper, R.; von Schnerin H. G. *Angew. Chem.* **1986**, *98*, 111. (c) von Schnering, H. G. *Z. Kristallogr.* **1986**, *174*, 182.
(67) Chen, B.; Eddaoudi, M.; Hyde, S. T.; O'Keefe, M.; Yaghi, O. M. *Science* **2001**, *291*, 1021.
(68) Von Schnering, H. G.; Nesper, R. *Angew. Chem., Int. Ed. Engl.* **1987**, *26*, 1059.
(69) Horner, M. A.; Ward, M. D. *CrystEngComm* **2004**, *6*, 401.
(70) Simonov, Y. A.; Malinovskii, S. T.; Bologa, O. A.; Zavodnik, V. E.; Andrianov, V. I.; Shibanova, T. A. *Kristallografiya* **1983**, *682*, 1983.
(71) MacGillivray, L. R.; Atwood, J. L. *Nature* **1997**, *389*, 469.
(72) Motherwell, W. D. S. *Acta Cryst.* **1997**, *B53*, 726.
(73) De Gelder, R.; Janner, A. *Acta Cryst.* **2005**, *B61*, 287.

crystals, suggesting further studies aimed at uniting the behavior of molecular crystals and soft matter is warranted.

Experimental Section

Materials and Methods. Reagents were used as received from the following commercial sources: ethylbenzene, anisole, and *m*-xylene (Acros Organics); 4-nitrobenzenesulfonic acid (Kodak); chloroform, methylene chloride, and toluene (Fisher); 1,2,3-trimethylbenzene and 1,2,3,4-tetramethylbenzene (TCI America); benzenesulfonic acid, chlorosulfonic acid, substituted benzenesulfonyl chlorides, starting materials used to prepare the organosulfonates other than those listed above, and guests other than those listed above (Aldrich). Methanol, the principal crystallization solvent, was used as received from Pharmco (ACS grade). Crude GMS salts were prepared by combining acetone solutions of guanidinium tetrafluoroborate and a select organomonosulfonic acid, which produced a crystalline precipitate of the corresponding white or off-white guest-free GMS compound. Single crystals of the guest-free GMS compounds for all 24 organomonosulfonates in Scheme 1 were obtained either by slow cooling or slow evaporation (at room temperature) of saturated methanol solutions. Except for G4SBBS, which formed extremely thin sheets that diffracted poorly, these procedures produced crystals suitable for single-crystal XRD analysis. GMS inclusion compounds with the general formula GMS·*n*(guest) were prepared either by slow cooling or evaporation of methanol solutions of a particular GMS compound and a guest selected from the right side of Scheme 1. This typically was achieved by dropwise addition of approximately 0.75 mL of guest to approximately 4 mL of methanol solution saturated with the GMS salt. This mixture was heated to dissolve any precipitate that formed, and then cooled to room temperature, typically producing crystals within 1 day. In cases where crystals did not appear, the solution was allowed to evaporate slowly at room temperature, which usually produced crystals of the inclusion compound within days. Alternatively, inclusion compounds of guests that were liquids at room temperature (guests 1−24) could be grown by slow diffusion of a methanol solution of a GMS salt across a layer of neat methanol covering the neat liquid guest. This method usually produced high-quality single crystals at the interface of the methanol solution and liquid guest. The stoichiometries of GMS guest inclusion compounds were determined by ^{1}H NMR in DMSO-d_6 (Varian INOVA 300 MHz spectrometer) and thermogravimetric analysis (Perkin-Elmer TGA 7). Crystal morphologies were characterized with an Olympus stereoscope (SZH10).

Synthetic Procedures. The organomonosulfonates in Scheme 1 were either available commercially, synthesized by sulfonation of commercially available arenes, or synthesized by hydrolysis of arene sulfonyl chlorides, depending upon the availability of starting materials. The syntheses of three representative guanidinium organomonosulfonates, each made by one of these approaches, are described here. The detailed syntheses of the remaining guanidinium salts formed with the organomonosulfonates in Scheme 1 are provided in the Supporting Information.

Commercially Available Sulfonic Acids*:* Guanidinium Benzenesulfonate (GBS). Benzenesulfonic acid (7.03 g, 44.44 mmol, Aldrich 90%) was dissolved in acetone (25 mL) and added to an acetone solution (50 mL) of guanidinium tetrafluoroboric acid (9.79 g, 1.5 equiv). After being cooled in the freezer the precipitate was filtered and washed with cold acetone to obtain guanidinium benzenesulfonate as a white crystalline solid (4.07 g, 42.2%). The filtrate was placed in the freezer overnight, and additional crystalline solid was harvested (1.12 g)(5.19 g, 53.8% overall); mp 214−218 °C. ^{1}H NMR (300 MHz, [D_6]DMSO): δ 7.59−7.63 (m, 2H), 7.31−7.33 (m, 3H), 6.93 (s, 6H).

Sulfonation of Arenes: Guanidinium 4-Isopropylbenzenesulfonate (G4IPBS). Chlorosulfonic acid (10.66 g 1.1 equiv) was added dropwise to a chloroform solution (100 mL) of isopropylbenzene (10.00 g, 83.20 mmol) over a period of 10 min, and the mixture was stirred at room temperature for 2 h. The solvent was removed under reduced pressure to obtain 4-isopropylbenzenesulfonic acid as a brown oil, which was dissolved in acetone (50 mL). An acetone solution (25 mL) of guanidinium tetraflouroborate (18.3 g, 1.5 equiv) then was added, producing guanidinium 4-isopropylbenzenesulfonate as a white crystalline solid (6.78 g 31.5%); mp 276−280. ^{1}H NMR (300 MHz, [D_6]-DMSO): δ 7.49−7.53 (m, 2H), 7.17−7.20 (m, 2H), 6.95 (s, 6H), 2.83−2.91 (m, 1H), 1.15−1.20 (m, 6H).

Hydrolysis of Sulfonyl Chlorides: Guanidinium 2-Methylbenzenesulfonate (G2MBS). *o*-Toluenesulfonyl chloride (5.08 g, 26.65 mmol) was dissolved in a mixture of dioxane (50 mL) and water (50 mL) and heated under reflux for 6 h. The solvent was removed under reduced pressure to produce 2-methylbenzenesulfonic acid as a brown oil. The oil was dissolved in 25 mL of acetone and mixed with guanidinium tetrafluoroboric acid (5.87 g, 1.5 equiv) dissolved in 25 mL of acetone. This mixture was chilled in a freezer, which afforded a precipitate that was filtered and washed with cold acetone to produce guanidinium 2-methylbenzenesulfonate as a white crystalline solid (4.39 g, 70.9%); mp 221−224 °C. ^{1}H NMR (300 MHz, [D_6]DMSO): δ 7.72 (d, 1H), 7.13−7.21 (m, 3H), 6.97 (s, 6H), 2.09 (s, 9H).

Crystallography. Single-crystal X-ray diffraction characterization was performed in the Department of Chemistry at the University of Minnesota. Experimental parameters and crystallographic information pertaining to the single-crystal X-ray analyses are given in Tables S1 and S2 (see Supporting Information). Full structure solutions were obtained by collecting a hemisphere of data on either Siemens or Bruker SMART CCD platform diffractometers with graphite monochromated Mo Kα radiation (l = 0.71073 A) at 173(2) K. The structures were solved by direct methods and refined with full-matrix least-squares/difference Fourier analysis using the SHELXTL package (*Structure Analysis Program 5.1*; Bruker AXS, Inc.: Madison, WI, 1997). All non-hydrogen atoms were refined with anisotropic displacement parameters and all hydrogen atoms were calculated and placed in idealized positions and refined with a riding model. Data were corrected for the effects of absorption using the Siemens area detector absorption program (SADABS). Unit-cell determinations were made by refinement on three sets of 20 matrix frames. Powder X-ray diffraction analysis was performed on either a Bruker-AXS (Siemens) D5005 or a Siemens D500 diffractometer.

Acknowledgment. This work was supported by the National Science Foundation (Grant DMR-0305278/0720655). The authors thank Victor G. Young, Jr. and William Brennessel of the X-ray Crystallographic Laboratory in the Department of Chemistry at the University of Minnesota for assistance with single-crystal X-ray structural analysis.

Supporting Information Available: X-ray experimental details in the form of crystallographic information file (CIF); crystallographic information for 39 new guest-free guanidinium organomonosulfonates and guanidinium organomonosulfonate inclusion compounds (Tables S1 and S2). This material is available free of charge via the Internet at http://pubs.acs.org.

JA0741574